



저작자표시-비영리-변경금지 2.0 대한민국

이용자는 아래의 조건을 따르는 경우에 한하여 자유롭게

- 이 저작물을 복제, 배포, 전송, 전시, 공연 및 방송할 수 있습니다.

다음과 같은 조건을 따라야 합니다:



저작자표시. 귀하는 원저작자를 표시하여야 합니다.



비영리. 귀하는 이 저작물을 영리 목적으로 이용할 수 없습니다.



변경금지. 귀하는 이 저작물을 개작, 변형 또는 가공할 수 없습니다.

- 귀하는, 이 저작물의 재이용이나 배포의 경우, 이 저작물에 적용된 이용허락조건을 명확하게 나타내어야 합니다.
- 저작권자로부터 별도의 허가를 받으면 이러한 조건들은 적용되지 않습니다.

저작권법에 따른 이용자의 권리는 위의 내용에 의하여 영향을 받지 않습니다.

이것은 [이용허락규약\(Legal Code\)](#)을 이해하기 쉽게 요약한 것입니다.

[Disclaimer](#)

Evaluation of internal adaptation on resin composite using micro-CT and SS-OCT



Seung Hoon Han

The Graduate School
Yonsei University
Department of Dentistry

Evaluation of internal adaptation on resin composite using micro-CT and SS-OCT

Directed by Professor Sung-Ho Park

A Dissertation Thesis

Submitted to the Department of Dentistry
and the Graduate School of Yonsei University

in partial fulfillment of the
requirements for the degree of
Doctor of Philosophy of Dental Science

Seung Hoon Han

December 2015

This certifies that the dissertation thesis of Seung Hoon Han is approved.

Thesis Supervisor: Sung-Ho Park

Thesis Committee Member #1: Byoung-Duck Roh

Thesis Committee Member #2 : Jeong-Won Park

Thesis Committee Member #3 : Kyoung-Nam Kim

Thesis Committee Member #4: Kwang-Mahn Kim

The Graduate School

Yonsei University

December 2015

Acknowledgements

For guiding my research and dissertation, I would like to express the deepest gratitude to my advisor, Prof. Sung-Ho Park. He has encouraged, supported and advised me during my entire program. He is my role model of a true teacher and has inspired me to be more professional.

To Prof. Byoung-Duck Roh I owe special thanks for his review and supporting my work. He encouraged me to start the post graduate program. I am grateful to Prof. Jeong-Won Park for his kind review in spite of his busy schedule. He has been my mentor since I was an undergraduate student. I would like to express my profound gratitude to Prof. Kyoung-Nam Kim for all his indispensable advice and I also wish to thank Prof. Kwang-Mahn Kim for his detailed advice on my thesis. I wish that I shall have a good relationship for future co-work researches.

I also want to thank Prof. Chan-Young Lee, Prof. Seung-Jong Lee, Prof. Il-Young Jung, Prof. Eui-seong Kim, Prof. Su-Jung Shin for their help and support. Without my teachers, I could not have finished my graduate course. My special appreciation goes to Prof. Junji Tagami, who was the dean of Tokyo Medical Dental University, for his help and advice. I also owe thanks to Prof. Alireza Sadr, who is a professor in University of Washington, for his continuous support of our research.

I wish to thank everyone in the department of conservative dentistry for their help. I have to apologize to all those colleagues who were not mentioned with their names.

Finally, I wish to dedicate this work to Young-Eun Lee, my wife. Without the support of my family, I could not have completed my graduate program. I really appreciate it with my heart. Thank you so much.

December, 2015

By Author

Table of Contents

List of figures and tables	ii
Abstract	1
I. Introduction	5
II. Materials, methods and results	10
1.1. The first experiment of evaluation on internal adaptation	10
1.2. The materials and methods of the first experiment	10
1.3. The results of the first experiment	18
2.1. The second experiment of evaluation on internal adaptation	19
2.2. The materials and methods of the second experiment	20
2.3. The results of the second experiment	30
3.1. The third experiment of evaluation on internal adaptation	34
3.2. The materials and methods of the third experiment	35
3.3. The results of the third experiment	43
III. Discussion	45
IV. Conclusion	52
References	53
Abstract in Korean	59

List of Figures

Fig. 1	Experimental procedure of this study	13
Fig. 2	SS-OCT image showing a microgap on the cavity floor	15
Fig. 3	Micro-CT image showing a microgap on the cavity floor	16
Fig. 4	Negative control image of SS-OCT	17
Fig. 5	Negative control image of micro-CT	18
Fig. 6	Tooth preparation from mesial view	21
Fig. 7	Bulk-fill resin placement and the locations of micro-CT scanning	22
Fig. 8	Measurement of imperfect margin for BWIM%, LWIM%, and GFIM% on the micro-CT	26
Fig. 9	Measurement of imperfect margin for MPFIM% and DPFIM% on the pulpal floor of the cavity	27
Fig. 10	Linear regression analysis of polymerization stress and TIM%	33
Fig. 11	Linear regression analysis of polymerization shrinkage and TIM%	34
Fig. 12	Experimental procedure	35
Fig. 13	SS-OCT image of High C-factor cavity with the inset of GapAnalyzer image ...	40
Fig. 14	SS-OCT image of Low C-factor cavity with the inset of GapAnalyzer image ...	41

List of Tables

Table 1	Percentages of defective margins (%DS) measured by SS-OCT and micro-CT	19
Table 2	Compositions of resin composites in this study	21
Table 3	Physical properties of resin composite in this study	31
Table 4	Two-way ANOVA results : Tests of Between-Subjects Effects	31
Table 5	Internal adaptation depending on its cavity location : Result of one-way ANOVA	32
Table 6	Internal adaptation of depending on its group (TIM%) : Result of one-way ANOVA	32
Table 7	Mean percentage of measured imperfect margin of each cavity wall or floor	32
Table 8	Compositions of composite resins used in this study	37
Table 9	Measurements of polymerization shrinkage and stress on resin composites used in this study	44
Table 10	Percentages of imperfect margin for each group	44
Table 11	Pearson Correlations Among Variables	44

Abstract

Evaluation of internal adaptation on resin composite using micro-CT and SS-OCT

Seung Hoon Han

Department of Dentistry

The Graduate School, Yonsei University

Directed by Professor Sung-Ho Park

I. Introduction

Internal adaptation, which means how well a restoration adapts to tooth material inside, can involve the evaluation of a microgap at the pulpal floor of a restoration. As a non-destructive method for evaluation of internal adaptation, micro-CT was introduced to evaluate the internal adaptation of restorations. For another method, optical coherence tomography (OCT) came to be used as a non-invasive cross-sectional imaging method for biological systems. A specific type of

OCT is a swept-source optical coherence tomography (SS-OCT).

The theme of this thesis is the evaluation of the internal adaptation on resin composite in different cavity configuration. This paper includes three different experiments on internal adaptation of resin composite using micro-CT and/or SS-OCT.

II. Materials, methods and results

1. The first experiment of evaluation on internal adaptation

Materials and Methods: Two cylindrical cavities were created on the labial surface of twelve bovine incisors. The 24 cavities were randomly assigned to four groups of dentine adhesives; 1) three-step etch-and-rinse adhesive, 2) two-step etch-and-rinse adhesive, 3) two-step self-etch adhesive, and 4) one-step self-etch adhesive. After application, the cavities were filled with resin composite. All restorations underwent a thermo-cycling challenge, and then, eight SS-OCT images were taken using a Santec OCT-2000™ (Santec Co., Komaki, Japan). The internal adaptation was also evaluated using micro-CT (Skyscan, Aartselaar, Belgium). The image analysis was used to calculate the percentage of defective spot (%DS) and compare the results. The groups were compared using one-way ANOVA with Duncan analysis at the 95% significance level. The SS-OCT and micro-CT measurements were compared with a paired t-test, and the relationship was analyzed using a Pearson correlation test at the 95% significance level.

Results: After thermo-cycling, the %DS results showed that Group 3 \leq Group 4 < Group 1 \leq Group 2 on both SS-OCT and micro-CT images. The %DSs on micro-CT were lower than those of SS-OCT ($p < 0.05$) and the Pearson correlation coefficient between SS-OCT and micro-CT was $r = 0.787$ ($p < 0.05$).

2. The second experiment of evaluation on internal adaptation

Materials and Methods: Standardized MOD cavities were prepared in 40 extracted human third molars. They were randomly divided into five groups (n=8). After being applied by dentin adhesive, the teeth were restored with the following resin composites: Group 1- Filtek Z350 (3M); Group 2- SDR (Dentsply) + Z350; Group 3- Venus Bulk Fill (Heraeus Kulzer) + Z350; Group 4- Tetric N-ceram bulkfill (Ivoclar Vivadent); and Group 5- SonicFill (Kerr). After thermo-mechanical load cycling, micro-CT images were taken cross-sectionally. Internal adaptation was measured as imperfect margin percentage (IM%). IM% is the percentage of defective margin length to the whole margin length. On the micro-CT images, IM% was measured at five interfaces to compare the differences. Linear polymerization shrinkage and polymerization stress were measured on each composite. To verify the correlation of polymerization stress and IM%, regression analysis was used.

Results: IM% on the cavity floors were higher than those of the cavity walls. IM% showed as Groups 4, 5 ≤ Groups 1, 2 ≤ Group 3 ($p < 0.05$). The relationship between polymerization stress and IM% was found to be $R^2 = 0.636$. The relationship between linear polymerization shrinkage and IM% turned out to be $R^2 = 0.618$.

3. The third experiment of evaluation on internal adaptation

Materials and Methods: Cylindrical cavities 3 mm in diameter were prepared in 100 human third molars in two depths; 4 mm (high C-factor: H-CF) or 1 mm (low C-factor: L-CF). After adhesive application (Clearfil SE One, Kuraray Noritake), the composite was placed in two increments in 3 subgroups: Filtek Supreme (FS, 3M ESPE); Charisma Diamond (CD, Heraeus Kulzer); Amelogen Plus (AP, Ultradent); and as a single increment in 2 subgroups; Tetric EvoCeram Bulk Fill (TB, Ivoclar Vivadent) and Venus Bulk Fill (VB, Heraeus Kulzer). After thermo-mechanical load-cycles, imperfect margin percentage (%IM) was calculated using optical coherence tomography (SS-OCT) imaging. The relationships between %IM and linear shrinkage (LS) and shrinkage stress, measured under either zero-compliance (PS0) or compliance-allowed (PS) conditions were evaluated.

Results: %IM was significantly different between H-CF and L-CF groups. The %IM in H-CF

turned out to be as: groups 2, 1 \leq group 4 < groups 3, 5. The %IM in L-CF showed as the following: groups 2, 4 \leq groups 1, 3 < group 5. There were significant correlations between shrinkage parameters and %IM, except between PS0 and %IM in L-CF.

III. Conclusion

Micro-CT and SS-OCT could be used as non-destructive methods for evaluation on the internal adaptation of composite restoration. Measured imperfect margin percentage (%IM) in micro-CT showed different values to those of SS-OCT, however, these two methods were relatively highly correlated. Self-etching adhesive systems showed fewer defective spots than etch-and-rinse adhesive systems in class I cavity.

At the gingival floor of the proximal box and pulpal floor of the cavity, flowable bulk-fill resin showed an inferior internal adaptation when compared with non-flowable ones. For Class II resin restorations, bulk-filling material of the non-flowable type could be preferable to flowable type ones. Polymerization shrinkage and stress, which was measured under the compliance-allowed setup, showed some relation to the internal adaptation.

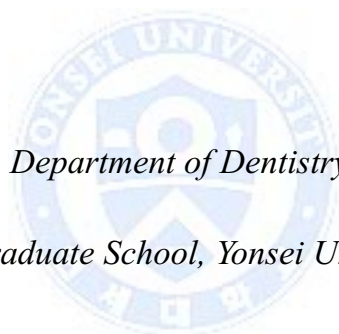
Within the limitations of the present study, it was shown that a higher imperfect margin percentage was found in the cavities of the High C-factor group. Internal adaptation was different depending on the composite material. Internal adaptations both in the High and Low C-factor cavities are correlated with polymerization stress measured under the compliance-allowed condition. In the Low C-factor cavity group, the polymerization shrinkage stress measured under the zero-compliance condition did not show a significant correlation to internal adaptation.

Keywords

internal adaptation, micro-CT, SS-OCT, optical coherence tomography, C-factor, polymerization shrinkage, polymerization stress, compliance, bulk-fill composite, dentin adhesive

Evaluation of internal adaptation on resin composite using micro-CT and SS-OCT

Seung Hoon Han



Department of Dentistry

The Graduate School, Yonsei University

Directed by Professor Sung-Ho Park

I. Introduction

Internal adaptation, which means how well a restoration adapts to tooth material inside, can involve the evaluation of a microgap at the pulpal floor of a restoration. It may be in relation to hypersensitivity to cold or pain on mastication (Eick and Welch, 1986). If the evaluation could not

be done with a non-destructive method, the specimen should be cut to be examined. This might lead to the interfacial leakage values becoming too high and may not be able to be evaluated repeatedly (Alani and Toh, 1997). The number of sectioned specimens is also very limiting, which may not be representative of the whole specimen (Braga et al., 2006; Braga and Ferracane, 2004). As a non-destructive method for evaluation of internal adaptation, micro-CT was introduced to evaluate the internal adaptation of restorations (De Santis et al., 2005; Kim and Park, 2014). For another method, optical coherence tomography (OCT) came to be used as a non-invasive cross-sectional imaging method for biological systems. After a laser source is projected over a restoration, the backscattered light is transformed into a signal intensity that can be shown as an image. OCT is a non-invasive method that can be used for different purposes such as detecting dental caries or cracks. A specific type of OCT is a swept-source optical coherence tomography (SS-OCT), which is known to have a better image resolution and scanning speed.

Microfocus X-ray computed tomography (micro-CT) is another useful method to evaluate the internal adaptation of restorations (De Santis et al., 2005). Recently, Kwon and Park proposed a method in which silver nitrate was penetrated from the pulp space through the dentinal tubules, and the amount of silver nitrate penetration was assessed by micro-CT (Kwon and Park, 2012). The authors reported it as a new measuring method for evaluating the internal adaptation without any destruction. In another study, the internal adaptation of dentin-composite was analyzed using micro-CT, and the correlation of internal adaptation with polymerization shrinkage was evaluated (Kim and Park, 2014). Due to the penetrating ability of X-rays, micro-CT enables the evaluation of dental hard tissue irrespective of its depth.

The OCT system has been utilized to investigate the cavity floor for the evaluation of internal adaptation. On the OCT image, interfacial microgap is observed as bright spot or line with high signal intensity (Bakhsh et al., 2011; Senawongse et al., 2011). The change in the signal intensity at the interface appears as a white cluster on the image. When light passes the interface between two media with different refractive indices, a portion of light is reflected. This is known as the Fresnel phenomenon and depends on the incidence angle and refractive index (n). The refractive index of air is 1.0 (n) and that of a tooth or resin composite is 1.5-1.6 (n) (Meng et al., 2009). If

there is a microgap formed by incomplete adhesion, air or water may exist at the interface. When light transverses the air at the interface, a portion of light is reflected and the OCT system shows a higher signal intensity. If the microgap is filled with another medium, such as water 1.33 (n), the reflection would not be as strong as that of the air.

In the past few years, new composite resins for the bulk fill technique have been introduced. Manufacturers suggested that resin restoration could be built up to 4-5 mm thick increment to be cured at one time. Bulk fill resin can be divided into two categories: flowable and non-flowable. The first bulk-fill materials on the market, SDR (Dentsply), Venus Bulk Fill (Heraeus Kulzer), x-tra base (Voco), and Filtek Bulk Fill (3M ESPE) were recommended to finish the restoration by adding a capping layer of a conventional composite resin (Ilie et al., 2013). On the other hand, other bulk fill resins like SonicFill (Kerr), Tetric EvoCeram Bulk Fill (Ivoclar Vivadent), and x-tra fil (Voco) can be placed without a capping layer. SonicFill can be placed with the help of a sonic-activated handpiece.

Researches have been done to evaluate the microleakage of bulk-fill composite resin restorations (Campos et al., 2014; Moorthy et al., 2012; Roggendorf et al., 2011). Moorthy et al. evaluated the cuspal deflection and cervical microleakage on the margins of Class II cavities which had been incrementally filled with composites or bulk-fill flowable resins (Moorthy et al., 2012). They found that cuspal deflection was lower in bulk-fill flowable resin, whereas there was no difference between the two composites in the cervical microleakage. Roggendorf et al. evaluated marginal integrity of bonded composite resin fillings on MOD cavities with and without a bulk-fill flowable 4 mm base (Roggendorf et al., 2011). They inspected the marginal gap using SEM and found that there was no negative influence on the marginal quality when a 4mm layer of bulk-fill SDR was used. Campos et al. investigated the marginal adaptation of bulk-fill composite restorations on Class II MO cavities (Campos et al., 2014). They concluded that bulk-fill materials do not allow better marginal adaptation than a standard composite resin applied by simple layering techniques.

Since flowable resin was introduced to composite resin restorations, it has been questioned if the use of flowable resin as a base could be advantageous for resin restoration. The rheology of

flowable resin could allow a better adaptation to the cavity walls (Aggarwal et al., 2014). In respect to the role of flowable resin, there was a suggestion that a flowable resin layer could act as a stress absorbing intermediate layer (Chuang et al., 2004). Kwon and Park reported that flowable composites of low modulus of elasticity as the base material could reduce marginal defects in overlying composite restorations (Kwon et al., 2010). On the other hand, Braga et al. reported that using a flowable resin composite as a restorative material is not likely to reduce the effects of polymerization stress (Braga et al., 2003). From this point of view, it has been questioned if placing a base with bulk-fill resin of the flowable-type could show better internal adaptation at the resin-tooth interface or not.

The magnitude of the polymerization shrinkage stress is influenced by numerous factors. These factors can be divided into the cavity configuration factor and the material property factor. The cavity configuration factor includes cavity volume, C-factor, and compliance of the cavity wall. For the material property factor, there can be filler content of composite, matrix formulation, polymerization shrinkage, polymerization stress, elastic modulus, flow of the resin, and adherence of the resin to the wall (Braga et al., 2005; Braga and Ferracane, 2004; Goncalves et al., 2011; Goncalves et al., 2010). The configuration of cavity walls, which can be represented as C-factor, is one variable that should be considered. The compliance of the substrate to be bonded can affect stress development. Filler content in composite resin can be one of the factors; if the composite has high inorganic filler content, it will show low volumetric shrinkage and high stiffness (Goncalves et al., 2011; Goncalves et al., 2010). The amount of polymerization shrinkage and viscoelastic properties can also be the variables on shrinkage stress. Braga et al. indicated that volumetric shrinkage prevails over viscoelastic properties in determining contraction stress (Braga et al., 2005). The viscoelastic properties include its flow capacity and elastic modulus, both of which can be variable during polymerization (Boaro et al., 2010a). Low elastic modulus and viscous flow at the early stage of polymerization can reduce shrinkage stress. In conclusion, the interplay among these factors can decide the polymerization shrinkage stress.

The most frequent method of measuring contraction stress is to use the tensiometer, however, there is some controversy about the tensiometer method. One of the concerns of the tensiometer

can be the compliance of the testing system. There are two types of measurement systems: zero compliance setup and compliance-allowed (non-rigid) setup. Zero (or near-zero) compliance means that a feedback system exists during the polymerization shrinkage measurement. When the test system does not have a feedback system, it indicates that the compliance is allowed, where composite resin can shrink relatively freely. When contraction force is measured with a non-rigid setup, the shrinkage force can be dissipated through the components of the system. There are two different reports on the relationship to the C-factor with these two settings. When the rigid (zero or near-zero) compliance system was used, there was a direct relationship between the polymerization stress and C-factor value (Choi et al., 2000; Feilzer et al., 1987). If the non-rigid system was used, an inverse relationship between them could be found (Bouschlicher et al., 1997; Watts et al., 2003). These findings raised the questions of why there were two opposite results of relationship between the stress and C-factor and which one of the two measurement systems would be applicable to evaluating microleakage or internal adaptation.

C-factor, which is a ratio of non-bonded surfaces to bonded ones, can represent cavity configuration. The C-factor concept should be carefully applied to clinical practice. Cavity configurations have a much more complex geometry than the specimens used in an experimental test. When it comes to C-factor and microleakage, Uno et al. presented that there was no relationship between the C-factor and gap dimension in compomer restorations with different C-factors (Uno et al., 1999). Another report suggested that microleakage seemed to be related to a restoration's volume, but not to its C-factor (Braga et al., 2006). However, in their studies, samples of different C-factors, which were set by changing their volumes of composite, were compared to find out the difference in microleakage. To evaluate the influence on the microleakage by C-factor, it would be more reasonable to set composite restorations' shape and volume as identical.

The theme of this thesis is the internal adaptation of resin composite in different cavity configuration. This paper includes three different experiments on internal adaptation of resin composite. For each experiment, the parts of material-methods and results will be described in separate section.

II. Materials, methods and results

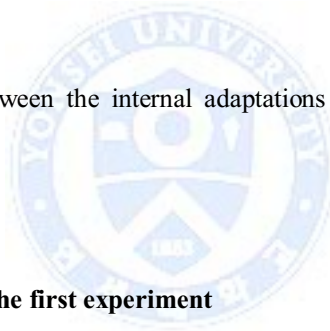
1.1. The first experiment of evaluation on internal adaptation

There are currently no comparative studies evaluating the two methods in the assessment of internal adaptation in composite restoration. The purpose of this study was to compare internal adaptation from SS-OCT and micro-CT. For this purpose, bovine cavities were restored with resin composite using different adhesive systems, and the internal adaptation was evaluated using SS-OCT and micro-CT.

The null hypotheses tested in the study were the following:

1) There is no difference in internal adaptation among the restorations in which different dentin adhesive systems are used

2) There is no difference between the internal adaptations measured by SS-OCT and those measured by micro-CT.



1.2. Materials and methods of the first experiment

1.2.1. Specimen preparation

This study used twelve extracted bovine mandibular incisors. The labial surface of each tooth was flattened with a trimmer and 600-grit sandpaper. Two round cylinder-shaped class I cavities (3 mm in diameter, 2 mm in depth) were made on the labial surface of each tooth. First, a flat-end tapered diamond bur attached to a high-speed air-turbine handpiece and a water coolant was used. Then, a cylinder-shaped stone point was used to create a standardized cavity.

The cavities were randomly assigned to four groups, each with six cavities. Two cavities in the same tooth were restored using the same adhesive system. The four groups were used to test four different materials as the dentin adhesive: Group 1, three-step etch-and-rinse adhesive (Scotch Bond Multipurpose, 3M, MN, USA); Group 2, two-step etch-and-rinse adhesive (Single bond 2,

3M, MN, USA); Group 3, two-step self-etch adhesive (Clearfil Megabond, known as Clearfil SE Bond outside Japan, Kuraray Noritake Dental, Tokyo, Japan); and Group 4, one-step self-etch adhesive (Clearfil SE One, Kuraray Noritake Dental, Tokyo, Japan). Each adhesive system was used according to the manufacturer's instructions. The adhesives were applied to the cavity surfaces, dried with gentle air and irradiated with a halogen light curing unit (Optilux 501, Kerr, CA, USA; 550 mW/cm²) for 10 seconds. The cavities were filled with the resin composite (Estelite Sigma Quick, Tokuyama Dental, Tokyo, Japan) using the bulk-filling technique and were light-cured for 40 seconds. The restorations were stored in 100% humid conditions at room temperature.

1.2.2. Thermo-cycling

All of the restorations underwent thermo-cycling (n=6 per group). A CS-4.8 chewing simulator (SD Mechatronik, Feldkirchen-Westerham, Germany) was used. The restoration underwent 100,000 thermo-cycles between 5°C and 55°C, with a dwelling time of 30 seconds in each temperature and a transferring time of 10 seconds.

1.2.3. Swept-source optical coherence tomography (SS-OCT)

The SS-OCT used in this study is the Santec OCT-2000™ (Santec Co., Komaki, Japan). It is a frequency domain OCT system integrating a high-speed frequency sweeping external cavity. The laser probe power is less than 20 mW. The light source in the system sweeps the wavelengths from 1260 nm to 1360 nm at a rate of 20kHz. The axial resolution of the OCT system is 11 μm in air, which is equivalent to 7 μm in a biological structure. A hand-held scanning probe connected to the SS-OCT was placed over the occlusal surface of the restorations and was oriented at a right angle to the occlusal surface of the restoration. The first SS-OCT image of a restoration was taken 100 μm from the mesial end of a cavity. Eight OCT images were taken for each restoration at intervals of 400 μm along the section of the restoration.

1.2.4. Silver nitrate infiltration & micro-CT imaging

All of the teeth were cut at the Cementoenamel junction (CEJ) to expose the pulp chamber. The restorations were soaked in 17% ethylenediamine tetraacetic acid (EDTA) for 5 min to remove the smear layer in the pulp chamber. The teeth were then rinsed with distilled water. The teeth were immersed in a 25% silver nitrate solution and were placed under 3.75 kPa pressure that was applied from the apical towards the pulpal side for 3 days. This step was performed to facilitate silver nitrate infiltration beneath the cavity floor. The restorations were then rinsed thoroughly with distilled water and stored in saline.

Eight cross-section images of micro-CT were taken for each restoration, and the images were extended from the mesial end of the cavity to its distal end at 400 μm pitch intervals. A high-resolution micro-CT (Model 1076, Skyscan, Aartselaar, Belgium) was used to obtain the images. The imaging settings were the following: acceleration voltage: 100 kV, beam current: 100 μA , Al filter: 0.5 mm, resolution: 18 μm and rotation: 360° in 0.5° steps. Two-dimensional sagittal images were obtained from each restoration. Each tooth was mounted on a special template that was exclusively designed for it. This template minimized the changes in the position of the restoration during repeated processes. The 2D images were analyzed using image analysis software (ImageJ™ ver. 1.45).

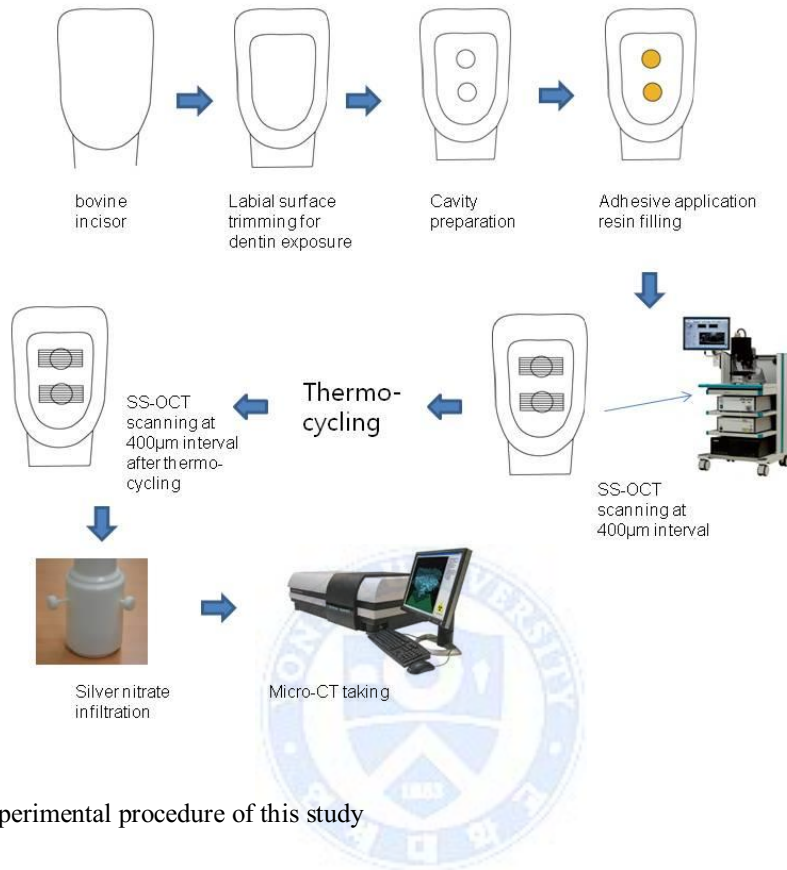


Fig. 1. Experimental procedure of this study

1.2.5. Image analysis

1.2.5.1. Preliminary study for negative control

The cavities of the same dimension were prepared on labial surface of bovine teeth as described before (n=4). Without priming or adhesive bonding, the same resin composite was filled and light cured. SS-OCT and micro-CT images were taken for negative control group (Figs. 4 and 5).

1.2.5.2. SS-OCT images analysis

The SS-OCT raw data were imported into the ImageJ™ program. The presence of air, which indicates a microgap within a defect, is visualized as bright areas in the SS-OCT images. It is known that when there is a microgap between two media of different refractive indices, the reflections of light at the interface will be dissimilar. The high signal intensity at the resin-dentin interface created bright spots or a line (Fig. 2). To measure the size of the bright spots, the image was subjected to a median filter to reduce the noise and then cropped to the area including the cavity floor. The cropped image of the cavity floor underwent a binarization process to determine which brightness level of pixels should be included. The image binarization process changes a grayscale image into a binary black-and-white image as previously described by Bakhsh et al (Bakhsh et al., 2011). The length of each bright spot was calculated after processing to binary image. To verify the leakage length of the floor, the function of plot profile in ImageJ™ was used. It could show signal intensity plot for rectangular selections. Bright spot or cluster was presented as high intensity value (Fig. 2 lower window). A part of cavity floor where signal intensity was above the threshold was thought to be imperfective margin.

The percentage of defective spots on the cavity floor (%DS) equals the sum of the bright spots or the cluster length / the length of the floor cavity x 100.

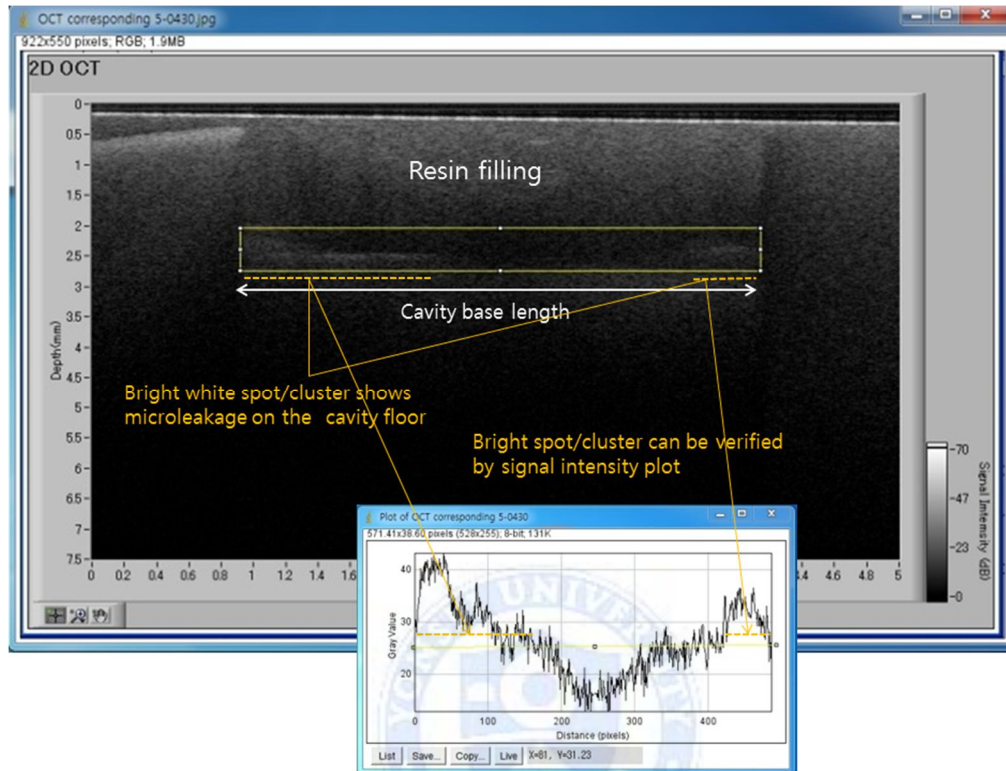


Fig. 2. SS-OCT image showing a microgap on the cavity floor

Lower window shows signal intensity plot for rectangular selection

1.2.5.3. Micro-CT images analysis

Eight images were obtained for each restoration at a 400 μm pitch, which was the same interval of the SS-OCT. The same evaluation method was used as that of the SS-OCT. The silver nitrate penetration into the microgap between the tooth and restorative material was identified by peaks of the graph on the plot profile function (Fig. 3 lower window). Using ImageJTM program for each restoration, the leakage spot or area was identified and measured as previously described for SS-OCT. All the leakage spots were summed per sample. The length of the leakage spots relative to

the whole cavity floor was calculated as percentage.

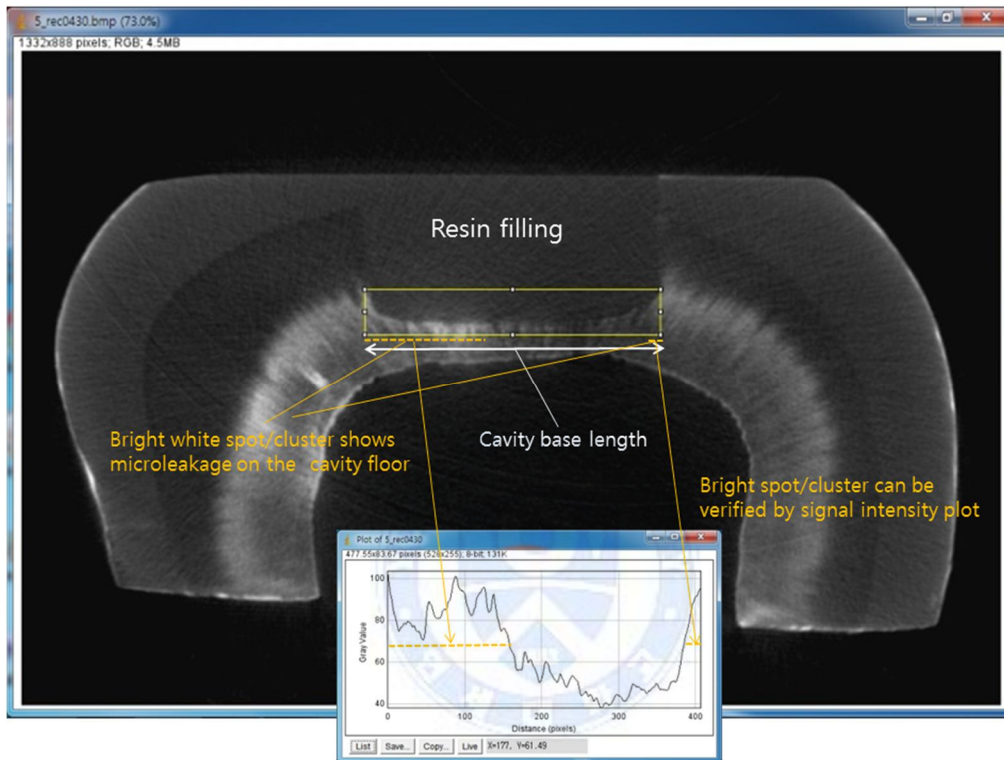


Fig. 3. Micro-CT image showing a microgap on the cavity floor after silver nitrate penetration

The white opaque band around pulp shows the dentinal tubules infiltrated by silver nitrate.

Lower window shows signal intensity plot for rectangular selection

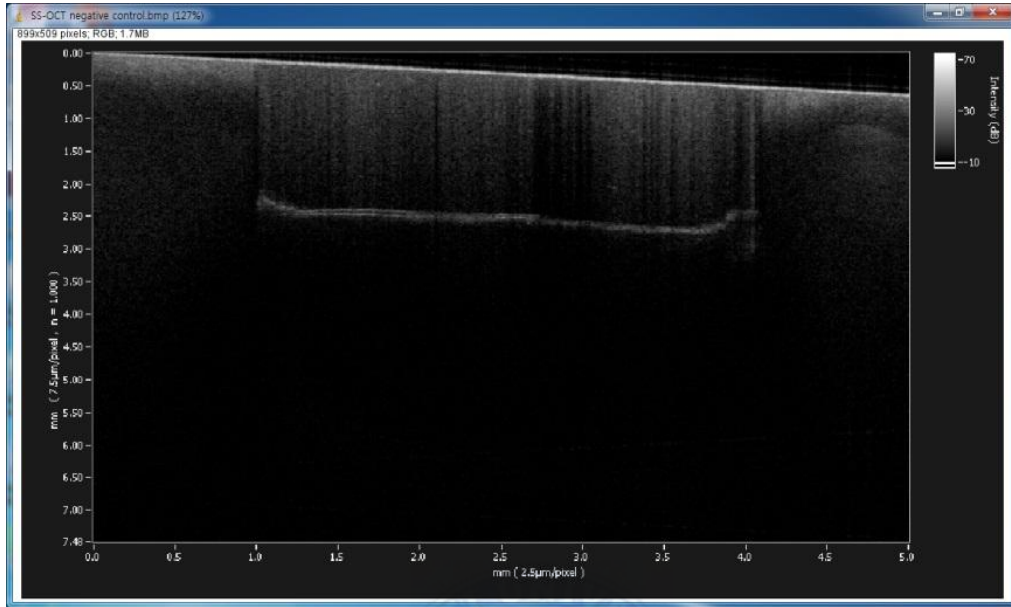


Fig. 4. Negative control image of SS-OCT



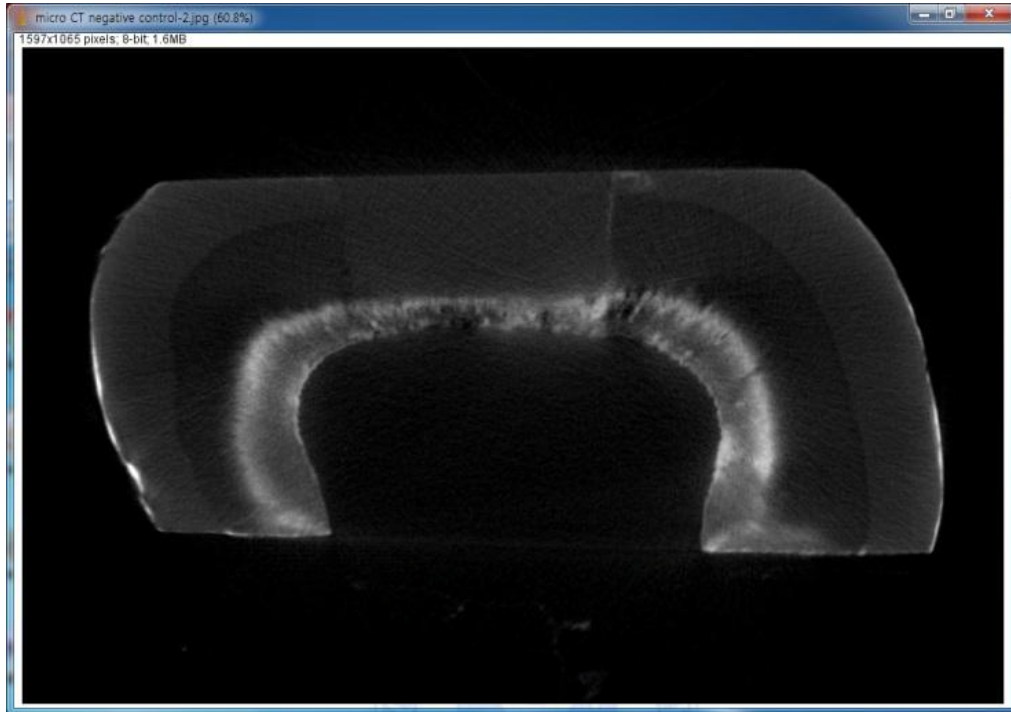


Fig. 5. Negative control image of micro-CT after silver nitrate penetration

1.2.6. Statistical analysis

The statistical analysis was conducted by PASW statistics 18 software (SPSS for windows: SPSS Inc., Chicago, IL, USA). Groups were compared using one-way ANOVA with Duncan's analysis at the 95% significance level. The SS-OCT %DSs before thermo-cycling was compared with the ones after thermo-cycling and the difference between %DSs of SS-OCT and micro-CT were also compared with a paired t-test and the relationship was analyzed using a Pearson correlation test at the 95% significance level.

1.3. The results of the first experiment

The results are presented in table 1. There was no difference in %DS among the groups before thermo-cycling. After thermo-cycling, %DSs identified by SS-OCT were significantly increased in all groups (closed bar with asterisk in table 1, $p<0.05$).

After thermo-cycling, the %DS of each group identified on both SS-OCT and micro-CT images could be sorted in the following increasing order; Group 3 \leq Group 4<Group 1 \leq Group 2.

The %DSs of the micro-CT imaging was lower than that of the SS-OCT, and the two groups were significantly different (table 1, $p<0.05$). The correlations of the two methods were also verified. The Pearson correlation coefficient between SS-OCT and micro-CT was $r=0.787$ ($p<0.05$).

Table 1. Percentages of defective margins (%DS) measured by SS-OCT and micro-CT

SS-OCT	Group 1	Group 2	Group 3	Group 4
Before thermo-cycling	35.21(7.6) ^{a *}	30.14(3.5) ^{a *}	28.88(5.1) ^{a *}	31.18(6.9) ^{a *}
After thermo-cycling	57.43(12.2) ^{a,b}	61.68(11.6) ^a	42.57(3.9) ^c	45.11(5.9) ^{b,c}
Micro-CT				
After thermo-cycling	30.49(4.7) ^{a,b}	31.09(6.6) ^a	22.46(3.1) ^c	23.08(4.0) ^{b,c}

Closed bar with asterisk indicates statistically significant difference before and after thermo-cycling ($p<0.05$).

Same superscript represents no statistically significant difference (compared in each row, one way ANOVA, $p<0.05$).

Values in the parenthesis represent standard deviations.

2.1. The second experiment of evaluation on internal adaptation

The second purpose of this study is to compare the internal adaptations of Class II resin restorations filled with different kinds of bulk-fill resins. This study investigated to see if there

would be any location-dependent differences or material-dependent differences. It also verified whether there would be any correlation between internal adaptation and polymerization shrinkage or stress.

The null hypotheses of this study were:

- 1) There was no difference in the internal adaptation of Class II composite restorations at the different locations of resin-tooth interfaces.
- 2) There was no difference in the internal adaptation of Class II composite restorations using different bulk-fill composite materials.
- 3) There was no correlation between the internal adaptation and the linear polymerization shrinkage or polymerization stress of the resin composite.

2.2. Materials and methods of the second experiment

2.2.1. Specimen preparation

Forty caries-free, sound lower third molars which had been extracted within three months were collected. The size of the specimen teeth was controlled as much as possible so that the differences in the bucco-lingual and mesio-distal length were less than 1 mm. After they were randomly divided into five groups, standard MOD cavities were prepared using diamond burs (959 KR 018, Komet, Germany). The cavity depth in the central fossa area was 4.5 mm and the bucco-lingual isthmus width was 3.5 mm. The proximal box of the cavity was prepared on the mesial side of the teeth. The cervical margin of the mesial proximal box was located 1 mm below the cemento-enamel junction (CEJ), while the cervical margin of the distal proximal surface was placed 1 mm above the CEJ. After tooth preparation, all the roots were resected at 2 mm below the CEJ (Fig.6).

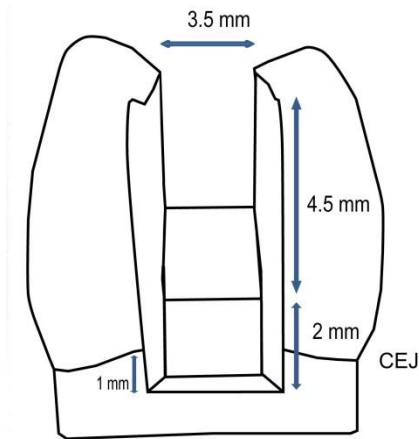


Fig. 6. Tooth preparation from mesial view

2.2.2. Base and composite filling

Table 2. Compositions of resin composites in this study

Code	Product	Manufacturer	Base resin	Filler (wt/vol.%)
Z3	Filtek Z350	3M ESPE, St Paul, MN, USA	Bis-GMA/EMA, UDMA	78.5/59.5 %
SD	SDR	Dentsply Caulk, Milford, DE, USA	Modified urethane dimethacrylate EBPADMA/TEGDMA	68/44 %
VB	Venus Bulk Fill	Heraeus Kulzer, Dormagen, Germany	UDMA, EBPADMA	65/38 %
TB	Tetric N-Ceram Bulk Fill	Ivoclar Vivadent, Schaan, Liechtenstein	Bis-GMA, UDMA dimethacrylate comonomers	78/55 % (including prepolymer)
SF	SonicFill	Kerr, West Collins, Orange, CA, USA	Bis-GMA, TEGDMA, EBPADMA	83.5/68 %

Composition and filler % were presented from manufacturer's information.

BIS-GMA: Bisphenol A glycidyl methacrylate.

BIS-EMA: Bisphenol A polyethylene glycol diether dimethacrylate.

UDMA: urethane dimethacrylate.

TEGDMA: Triethyleneglycol dimethacrylate.

The materials used in this study are shown in Table 2. According to the manufacturer's instructions, enamel margins were etched with 34% phosphoric acid (Caulk, Denstsply) for 15 s, irrigated with distilled water then air-dried. After XP bond (Dentsply Caulk, Milford, DE, USA) was applied to each cavity, light curing was done on the occlusal, mesial, and distal sides for 20 s each by an LED type light source (Bluephase, Ivoclar Vivadent, Schaan, Liechtenstein, 800 mW/cm²). Resin composite was placed after the adhesive treatment. Five different kinds of resin composites were used in this study.

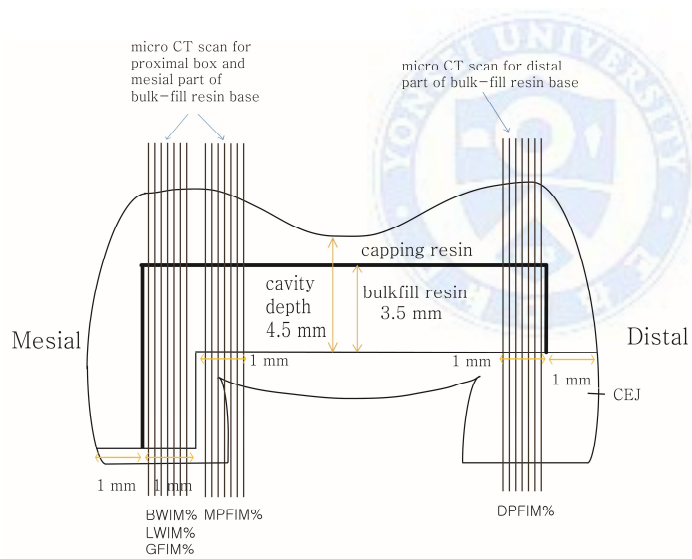


Fig. 7. Bulk-fill resin placement and the locations of micro-CT scanning

BWIM% = Buccal wall imperfect margin %, LWIM% = Lingual wall imperfect margin %, GFIM% = Gingival floor imperfect margin %, MPFIM% = Mesial pulpal floor imperfect margin %, DPFIM% = Distal pulpal floor imperfect margin %, CEJ=Cemento-enamel Junction.

1) Group 1 (Z3, Control group)

After application of the ivory retainer and matrix to the tooth specimen, Filtek Z350 composite resin (A3, 3M, St. Paul, MN, USA) was applied. The first 2 mm increment was placed in the mesial proximal box and was light-cured for 20 s from the occlusal side. The second and third 2 mm increments were placed in the mesial proximal box and onto the pulpal floor, then light-cured for 20 s each from the occlusal side. The fourth and fifth increments were placed in the mesial and distal half of the remaining cavity and were light-cured for 20 s each from the occlusal side. After removing the retainer and the matrix, additional light-curing was applied from the buccal and lingual sides of the mesial and distal cavities obliquely from the occlusal surface. Eighty seconds of additional light-curing (20 s x 2 for mesial side, 20 s x 2 for distal side) was applied in this process.

2) Group 2 (SD, flowable bulk-fill resin) and Group 3 (VB, flowable bulk-fill resin)

After being applied by an ivory retainer and matrix to the specimens, flowable bulk-fill resin was filled in each cavity in the base portion of the cavity. For Group 2, SDR (Dentsply Caulk, Milford, DE, USA) bulk-fill resin was put onto the mesial proximal box and light-cured. Then the resin was placed onto the pulpal floor 3.5 mm thick and light-cured (Fig. 7). For Group 3, Venus Bulk Fill (Heraeus Kulzer, Dormagen, Germany) was put and light-cured in the same way as Group 2. Light curing was done with an LED type light source for 20 s from the occlusal side. The base materials and cavity walls were trimmed with a fine diamond bur to control the thickness of the base. Z350 composite was added to the remaining cavity (first onto the mesial proximal, then onto the distal proximal, the mesial cusp portion, and the distal cusp portion). Light curing was done for 20 s after each application. After removing the retainer and the matrix, additional light-curing was applied from the buccal and lingual sides of the mesial and distal cavities obliquely from the occlusal surface. Eighty seconds of additional light-curing (20 s x 2 for mesial side, 20 s x 2 for distal side) was applied in this process.

3) Group 4 (TB, non-flowable bulk-fill resin) and Group 5 (SF, non-flowable bulk-fill resin).

After being applied by an ivory retainer and matrix to the specimens, non-flowable bulk-fill resin was filled in each cavity of Groups 4 and 5. For Group 4, Tetric N-ceram Bulk Fill (Ivoclar vivadent, Schaan, Liechtenstein) was put using hand instruments with the same dimension as that of Groups 2 and 3. It was followed by light curing for 20 s. Another layer of Tetric N-ceram Bulk Fill composite was added to the remaining cavity and light-cured in the same way as Groups 2 and 3. For Group 5, SonicFill (Kerr, West Collins, Orange, CA, USA) was filled with a sonically activated handpiece following the manufacturer's instruction. After SonicFill resin had been filled to the full depth of the cavity, light-curing was done for 20 s. After removing the retainer and the matrix, additional light-curing was applied from the buccal and lingual sides of the mesial and distal cavities obliquely from the occlusal surface. Eighty seconds of additional light-curing (20 s x 2 for mesial side, 20 s x 2 for distal side) was applied in this process.

2.2.3. Thermo-mechanical load cycling

After 24 h water storage, the specimens were mechanically loaded using chewing simulator CS-4.8 (SD Mechatronik, Feldkirchen-Westerham, Germany). They were thermo-cycled under thermodynamic conditions (5 °C -55 °C, with a dwell-time of 60 s and a transfer time of 24 s) and a mechanical load of 5 kgf (49 N) for 600,000 times simultaneously. The conical-shaped opposing plunger, which was made of nickel-chromium, was initially positioned at the center of the restoration. A 5 kgf load was applied from the top surface and pressed down to the center of the tooth. The rod moved 6 mm vertically and 0.3 mm horizontally. The rising speed was 55 mm/s, while the descending speed was 30 mm/s. After the thermo-mechanical loading, the samples were stored in distilled water at room temperature.

2.2.4. Silver nitrate infiltration

The specimens were soaked in 17 % ethylenediamine tetraacetic acid (EDTA) for 5 min to remove the smear layer in the pulp chamber. Then they were rinsed with distilled water. The teeth were immersed in a 25% silver nitrate solution and were placed under 3.75 kPa pressures, upside down, for 3 days. This step was carried out to facilitate silver nitrate infiltration from the pulp chamber into the cavity floor. The specimens were then rinsed thoroughly with distilled water and kept in water at room temperature.

2.2.5. Micro-CT imaging

Thirty micro-CT images were taken cross-sectionally of each specimen. Ten micro-CT images for the proximal box were taken extending from the mesial end of the bulk-filled base to the axial wall of the proximal box at 90 μ m pitch intervals. Another ten micro-CT images were taken at the mesial end of the bulk-filled cavity floor. The last ten micro-CT images were taken from the distal end of the bulk-filled base toward the center of the cavity at the same intervals (Fig. 7). High-resolution micro-CT (Model 1076, Skyscan, Aartselaar, Belgium) was used to obtain the images. The imaging settings were as follows: acceleration voltage, 100 kV; beam current, 100 μ A; Al filter, 0.5 mm; resolution, 18 μ m; and rotation, 360° in 0.5° steps. Each tooth was mounted on a special template exclusively designed for it. The 2D images were analyzed using image analysis software (ImageJ™ ver. 1.46).

2.2.6. Evaluation of internal adaptation

To evaluate the internal adaptation of the specimens, the silver spots which were present between tooth and restoration were measured on the micro-CT images. All the images were taken from the mesial point of view. Fig. 8 shows one of the images at the mesial proximal box and Fig. 9 shows another image taken at a non-proximal box portion of the cavity

The imperfect margin percentage (IM%) was calculated by dividing the sum of the portions where the silver nitrate had penetrated into the microgap by the entire length of a wall or floor. The local IM% was calculated for each image. On the proximal box images, the buccal wall imperfect margin % (BWIM%), lingual wall imperfect margin % (LWIM%), and gingival floor imperfect margin % (GFIM%) were measured (Figs. 7, 8). Mesial pulpal floor imperfect margin % (MPFIM%) was measured on the micro-CT images taken from mesial end of pulpal floor toward 1mm the center of the cavity (Figs. 7, 9). Distal pulpal floor imperfect margin % (DPFIM%) was measured on those taken from distal end of bulk-filled base.

To verify correlation of polymerization stress and the imperfect margin, the total imperfect margin % (TIM%) was calculated. TIM% was defined as the percentage calculated by dividing the sum of imperfect margins on the buccal wall, lingual wall, gingival floor, mesial pulpal floor, and distal pulpal floor by the sum of all the internal margins.

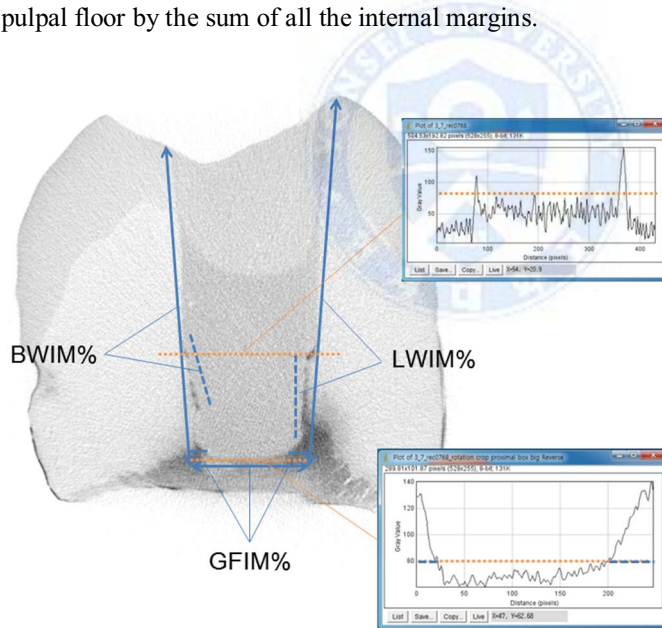


Fig. 8. Measurement of imperfect margin for BWIM%, LWIM%, and GFIM% on the micro-CT

BWIM% = Buccal wall imperfect margin %, LWIM% = Lingual wall imperfect margin %, GFIM% = Gingival floor imperfect margin %.

The plot profile shows the intensities of the pixels along the horizontal axis. The function of the plot profile in the ImageJ software shows gray density of the selected line or area. Dentin showed gray density at the 20-40 levels, the 40-70 levels in bulk-fill resin, and higher than the 80 level when silver nitrate infiltrated into the gap (right upper and lower windows). Intensity over 80 was regarded as a critical value to determine the imperfect area.

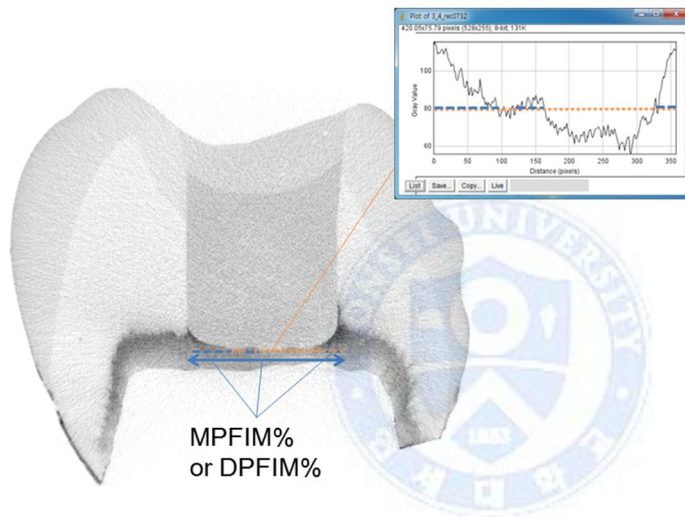


Fig. 9. Measurement of imperfect margin for MPFIM% and DPFIM% on the pulpal floor of the cavity

MPFIM% = Mesial pulpal floor imperfect margin %, DPFIM% = Distal pulpal floor imperfect margin %.

The plot profile shows the intensities of the pixels along the horizontal axis. Intensity over 80 was regarded as a critical value to determine the imperfect area.

The definitions of the terms are as follows:

BWIM% (Buccal wall imperfect margin %) = (the length of the buccal wall of the proximal box that was penetrated by silver nitrate/ the height of buccal wall of the proximal box) x 100

LWIM% (Lingual wall imperfect margin %) = (the length of the lingual wall of the proximal box that was penetrated by silver nitrate/ the height of lingual wall of the proximal box) x 100

GFIM% (Gingival floor imperfect margin %) = (the length of the gingival floor of the proximal box that was penetrated by silver nitrate/ the width of gingival floor of proximal box) x 100

MPFIM% (Mesial pulpal floor imperfect margin %) = (the length of the mesial pulpal floor of the occlusal cavity that was penetrated by silver nitrate/ the width of pulpal floor of the cavity) x 100

DPFIM% (Distal pulpal floor imperfect margin %) = (the length of the distal pulpal floor of the occlusal cavity that was penetrated by silver nitrate/ the width of pulpal floor of the cavity) x 100

TIM% (Total imperfect margin %) = (the sum of the imperfect margin measurements on the buccal wall, lingual wall, gingival floor, mesial pulpal floor, distal pulpal floor/ the total length of all internal margins) x100

2.2.7. Measuring polymerization linear shrinkage of resin composite

Polymerization shrinkage strain was measured using a custom-made Linometer (R&B Inc., Daejeon, Korea). Glycerin gel was applied to a metallic disc and a portion of a glass slide to prevent adhesion to the resin. Resin composites were measured in a custom Teflon mold to ensure that the same amount of composite resin (29.45 mm²; 5 mm diameter x 1.5 mm high disc) was used for each linometer sample. Then it was transferred onto the thin metallic discs, covered with a glass slide, and positioned into place under constant pressure using a screw. An LED type light-curing unit (Bluephase, Ivoclar Vivadent, Schaan, Liechtenstein) with a power density of 800 mW/cm² was placed 1 mm above the glass slide, and the material was light-cured for 30 s. As the resin composite under the glass slide was cured, it moved the aluminum disk upward. The amount of disc displacement, which was caused by the linear shrinkage of the resin composite, was measured

using an eddy current sensor every 0.5 s for a period of 180 s. This measurement was repeated five times for each material and the average was calculated (Table 3).

2.2.8. Measurement of the polymerization shrinkage force under a compliance-allowed condition

The polymerization shrinkage force of the resin composite was measured using a custom-made device and software (R&B Inc., Daejeon, Korea). The instrument was driven by a motor and was devised to move a load bar up and down. The polymerization shrinkage force applied to the bar was measured by a load cell (Model: UM-K100, capacity 100kgf, Dacell, Chungcheongbuk-do, South Korea) connected to the bar. The composite was placed between an acrylic disc, which was screwed into the load bar, and a transparent cylinder. The light to polymerize the resin composite was projected from beneath the transparent cylinder. The entire process was controlled by the software made by R&B Inc.

The surface of the acrylic disk was roughened with sandpaper before screwing it to the load bar. Then the surface was applied with adhesive resin (Bond, Clearfil SE Bond, Kuraray Noritake Dental, Okayama, Japan), and light-cured for 20 s. For the measurement of polymerization stress, a Teflon mold was used to measure the consistent amount of resin composite (7.07 mm²; 3 mm diameter x 1 mm high disc) The composite was placed onto the acrylic disc, and the load bar into which the disk was screwed was moved so that the dimension of the composite specimen was a 1 mm thick disk with a 3 mm diameter. Before measurements, the setup was switched to compliance-allowed mode in which the feedback system to control the original position of the load bar was not activated and the compliance of the system was 0.3 $\mu\text{m}/\text{N}$. The force between the tension rod and the resin composite was set to zero before light curing. Then the resin composite was light-cured with a light-curing unit (Bluephase, Ivoclar Vivadent, Schaan, Liechtenstein, 800 mW/cm²) through the transparent disc for 20 s. Along with the load-cell signal, the displacement was continuously recorded to the computer every 0.1 s for a period of 180 s. This measurement was repeated five times for each material and calculated for an average value (Table 3).

2.2.9. Statistical analysis

1) Comparison of IM%

Statistical analysis was done by PASW Statistics 18 software (SPSS for Windows: SPSS Inc., Chicago, IL, USA). To compare the internal adaptation, two-way ANOVA with Scheffe analysis was applied first. To compare the internal adaptations of different groups and those of different locations, one-way ANOVA with Scheffe analysis was used.

2) Analysis of relationship between polymerization shrinkage, stress, and IM%

TIM% was calculated per each specimen. All of the imperfect margin lengths were summed up. Then it was divided by all the internal margin lengths and multiplied by 100.

The following relationships between the measurement of polymerization stress and IM% were analyzed by regression analysis:

2-1) Polymerization stress versus TIM%

2-2) Linear polymerization shrinkage versus TIM%

2.3. The results of the second experiment

Table 3 shows flexural modulus, linear polymerization shrinkage, and polymerization shrinkage stress of resin composite in the study.

Table 3. Physical properties of resin composite in this study

Code	Flexural modulus (GPa)*	Linear polymerization shrinkage (%)	Polymerization shrinkage stress (MPa)
Z3	6.32 (0.65) ^d	1.36 (0.10) ^a	2.19 (0.12) ^{a,b}
SD	3.04 (0.63) ^c	1.78 (0.12) ^b	3.02 (0.17) ^c
VB	1.10 (0.15) ^a	2.27 (0.11) ^c	3.46 (0.18) ^d
TB	5.33 (0.43) ^c	1.20 (0.09) ^a	2.03 (0.12) ^{a,b}
SF	6.03 (0.45) ^{c,d}	1.21 (0.12) ^a	1.86 (0.15) ^a

Polymerization stress was calculated under compliance-allowed condition.

Identical letters within each column indicate no statistically significant difference between the groups, $p=0.05$.

*Flexural modulus measurements were adopted from the reference.(Jeong and Park, 2014)

Two-way ANOVA results showed that there was no interaction between filling materials and locations (Table 4, $p>0.05$). The results of groups compared by one-way ANOVA are presented in Tables 5 and 6. The results in Table 7 were compared by one-way ANOVA, horizontally (among different filling materials) and vertically (among different locations).

Table 4. Two-way ANOVA results : Tests of Between-Subjects Effects

Source	Type III Sum of Squares	df	Mean Square	F	Sig.
Corrected Model	1.283 ^a	24	.053	32.118	.000
Intercept	24.204	1	24.204	14538.199	.000
Group	.951	4	.238	142.795	.000
Location	.287	4	.072	43.132	.000
Group * location	.045	16	.003	1.696	.051
Error	.291	175	.002		
Total	25.779	200			
Corrected Total	1.575	199			

a. R Squared = .815 (Adjusted R Squared = .790)

**Table 5. Internal adaptation depending on its cavity location
Result of one-way ANOVA**

Location of interface	N	Subset	
		1	2
Lingual wall	40	26.2175	
Buccal wall	40	26.6197	
Distal pulpal floor	40		38.8276
Gingival floor	40		40.5827
Mesial pulpal floor	40		41.6917

**Table 6. Internal adaptation of depending on its group
Result of one-way ANOVA (TIM%)**

Group	N	Subset		
		1	2	3
5 (SF)	40	30.1221		
1 (Z3)	40	32.8954	32.8954	
4 (TB)	40	32.9378	32.9378	
2 (SD)	40		37.0317	37.0317
3 (VB)	40			40.9522

Table 7. Mean percentage of measured imperfect margin of each cavity wall or floor

	Z3	SD	VB	TB	SF
BWIM%	27.8 ^{a,A,B} (4.24)	28.3 ^{a,B,C} (4.07)	29.9 ^{a,C} (4.52)	24.4 ^{a,A,B} (5.03)	23.4 ^{a,A} (4.24)
LWIM%	25.2 ^{a,A,B} (5.94)	27.0 ^{a,B,C} (4.02)	29.7 ^{a,C} (3.48)	25.3 ^{a,A,B} (5.90)	23.9 ^{a,A} (3.6)
GFIM%	37.7 ^{b,A,B} (4.98)	43.4 ^{b,B,C} (3.33)	48.5 ^{b,C} (3.28)	38.9 ^{b,A,B} (5.29)	34.5 ^{b,A} (3.51)
MPFIM%	38.0 ^{b,A,B} (3.22)	45.1 ^{b,B,C} (3.11)	50.2 ^{b,C} (2.97)	40.1 ^{b,A,B} (2.85)	35.1 ^{b,A} (2.74)
DPFIM%	36.5 ^{b,A,B} (3.77)	41.3 ^{b,B,C} (4.14)	46.4 ^{b,C} (5.06)	36.2 ^{b,A,B} (3.30)	33.7 ^{b,A} (2.73)

BWIM% = Buccal wall imperfect margin %, LWIM% = Lingual wall imperfect margin %, GFIM% = Gingival floor imperfect margin %, MPFIM% = Mesial pulpal floor imperfect margin %, DPFIM% = Distal pulpal floor imperfect margin %.

Standard deviation in parentheses.

Lower case superscripts represent differences in IM% among the locations where the imperfect margin was measured in each group at $p < 0.05$ level (compared vertically).

Capital superscripts represent differences in IM% among the groups in each location at $p < 0.05$ level (compared horizontally).

Identical letters represent no statistical difference at $p < 0.05$ significance.

In all the groups, GFIM% (Gingival floor), MPFIM%, and DPFIM% (Pulpal floor) were significantly higher than BWIM% and LWIM% ($p < 0.05$). There was no significant differences among GFIM%, MPFIM%, and DPFIM% ($p > 0.05$) (Table 5). IM% of different groups were Groups 5, $1 \leq$ Groups 4, $2 \leq$ Group 3 (Table 6). The R^2 was 0.636 for polymerization stress versus TIM%, and it was 0.618 for linear polymerization shrinkage versus TIM% (Figs. 10 and 11).

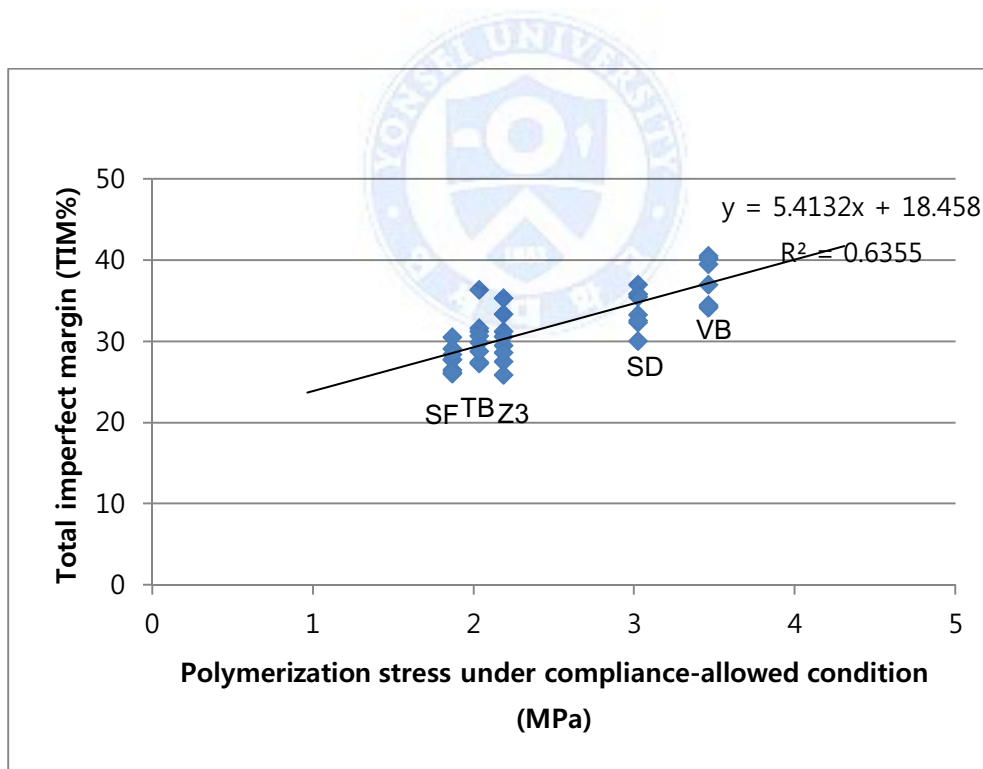


Fig. 10. Linear regression analysis of polymerization stress and TIM%

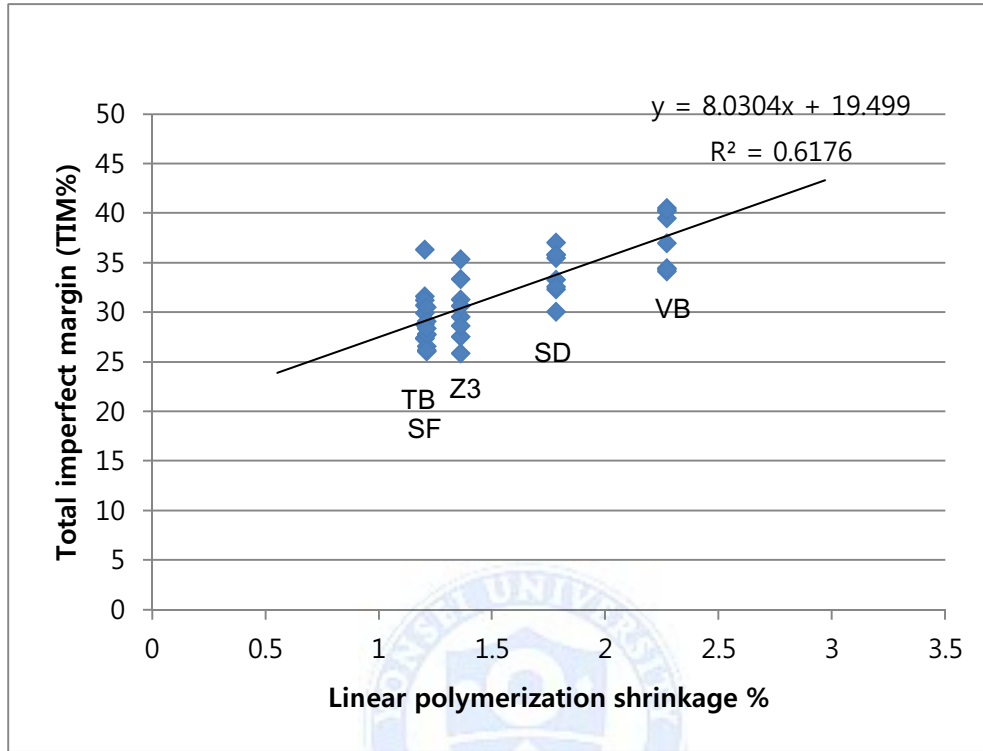


Fig. 11. Linear regression analysis of polymerization shrinkage and TIM%

3.1. The third experiment of evaluation on internal adaptation

The third purpose of this study was to compare the internal adaptations of different resin composites in two cavity configurations (High and Low C-factors) and to find out the relationship between the internal adaptation and polymerization shrinkage or shrinkage stress. The shrinkage stress was evaluated under zero-compliance and compliance-allowed conditions. In the present study, two cavities of different C-factors with the same volume and shape were prepared and restored with different composite resins. Then the internal adaptations were compared in two ways.

The null hypotheses were:

1. There was no difference in internal adaptation between High and Low C-factor cavities; and
2. There was no difference in internal adaptation among the different composite restorations in each High and Low C-factor cavity.

Additionally, the regression analysis between internal adaptation and linear polymerization shrinkage or polymerization stress was done in two different C-factors (High and Low C-factor cavities). The polymerization stress was measured both under a zero-compliance and a compliance-allowed condition.

3.2. Materials and methods of the third experiment

3.2.1. Experimental setup

The setup of this study is schematically illustrated in Fig. 12.

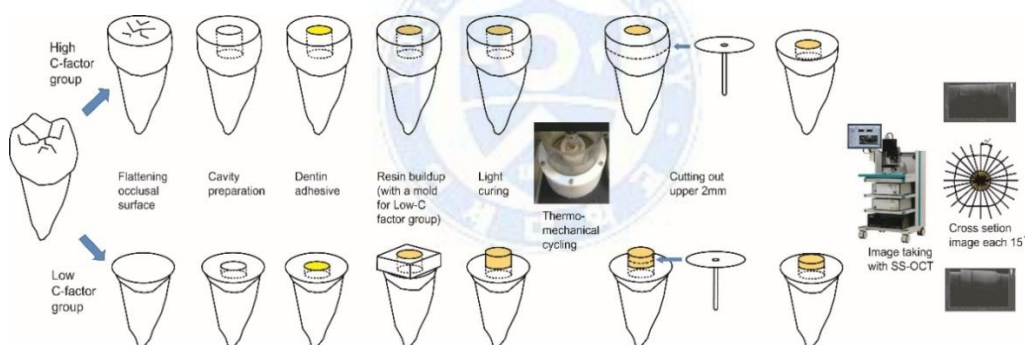


Fig. 12. Experimental procedure of this study

3.2.2. Specimen preparation

One hundred non-carious human third molars were used in this study. They were stored in 0.5 % chloramine solution for up to 2 months after extraction. The occlusal surface of each tooth was flattened with a trimmer and 320-grit sandpaper. All the teeth were randomly divided in two groups: High C-factor cylindrical cavity group and Low C-factor cylindrical cavity group. For the

High C-factor cylindrical cavity, round cylinder-shaped Class I cavities (3 mm in diameter, 4 mm in depth) were made on the occlusal surface of each tooth using a high-speed air-turbine handpiece with a flat-end tapered diamond bur (959 KR 018, Komet, Germany) under water coolant. Then the irregularities and cavity dimension were finely tuned using a low speed handpiece with a cylinder-shaped stone point (040 Dura green stone, Shofu, Japan) and hand instruments. For the Low C-factor cylindrical cavity, all the teeth were reduced 3 mm in height to the same depth of dentin as the High C-factor cavity before tooth preparation. The cavity bottom dentin in all the specimens was mid-coronal to make sure that the effects of regional variability would be negligible. Then round cylinder-shaped Class I cavities (3 mm in diameter, 1 mm in depth) were made on the occlusal surface of each tooth by the same methods as in the High C-factor cavity.

3.2.3. Resin composite filling

The High C-factor cavity group was divided into five subgroups (n=10) according to the composite used. A one-step self-etch adhesive (Clearfil SE One, Kuraray Noritake Dental, Tokyo, Japan) was used for dentin bonding. Following the manufacturer's instruction, the cavities were treated and light-cured. Composite filling materials included three kinds of hybrid composites and two bulk-fill types. The five subgroups of the High C-factor group were the following: Group H-CF-FS, which was filled with Filtek Supreme (3M, St. Paul, MN, USA); Group H-CF-CD with Charisma Diamond (Heraeus Kulzer, Dormagen, Germany); Group H-CF-AP with Amelogen Plus (Ultradent, South Jordan, UT, USA); Group H-CF-TB with Tetric Evoceram Bulk Fill (Ivoclar Vivadent, Schaan, Liechtenstein); and Group H-CF-VB with Venus Bulk Fill (Heraeus Kulzer, Dormagen, Germany). These cavities were filled either in bulk (H-CF-VB and H-CH-TB) or two equal increments of 2 mm as horizontal layers (H-CF-FS, H-CF-CD, and H-CF-AP). For the bulk filling groups, light-curing was done for 40 s with an LED curing device (Bluephase, Ivoclar Vivadent, Schaan, Liechtenstein; 800mW/cm²). For the incremental filling groups, light-curing was done twice for 20 s after each placement of hybrid composite. The resulting C-factor of the High C-factor cavity group was 6.33. The restorations were stored in distilled water at room temperature.

The Low C-factor cavity group was also divided into five subgroups (n=10). The same adhesive was applied to each specimen, dried, and light-cured. To make the specimens of equal volume, a custom silicone mold was used. The silicone mold has a hollow cylinder inside of which the internal dimension is 3 mm in diameter and 3 mm in height. After the mold was placed on the top of the occlusal surface, the same five subgroups as Group High C-factor were made. The Low C-factor group cavities were filled with composite either in bulk (L-CF-VB and L-CF-TB) or two equal increments of 2-mm horizontal layers (L-CF-FS, L-CF-CD, and L-CF-AP). For the bulk filling groups, light-curing was done for 40 s with the same LED curing device as in the High C-factor group. For incremental filling groups, light-curing was done twice for 20 s each after each placement of composite. After light-curing, the same dimension (3 mm in diameter, 4 mm in height cylinder) of restoration was obtained as that of the High C-factor cavity group. The resulting C-factor of the Low C-factor cavity group was 0.467. The restorations were stored in distilled water at room temperature.

Table 8. Compositions of composite resins used in this study

Code	Product	Manufacturer	Base resin	Filler (wt/vol.%)
FS	Filtek Supreme	3M ESPE, St Paul, MN, USA	Bis-GMA/EMA, UDMA	78.5/59.5%
CD	Charisma Diamond	Heraeus Kulzer, Dormagen, Germany	Bis-GMA	N.A/58%
AP	Amelogen Plus	Ultradent, South Jordan, UT, USA	Bis-GMA, TEGDMA	76/61%
TB	Tetric N-ceram bulkfill	Ivoclar Vivadent, Schaan, Liechtenstein	Bis-GMA, UDMA dimethacrylate co-monomers	78/55% (including prepolymer)
VB	Venus Bulk Fill	Heraeus Kulzer, Dormagen, Germany	UDMA, EBPDMA	65/38%

Base resin composition and filler % are the information from the manufactures.

3.2.4. Thermo-mechanical load cycling

After 24h water storage, the specimens were mechanically loaded using a chewing simulator

CS-4.8 (SD Mechatronik, Feldkirchen-Westerham, Germany). They were thermo-cycled under thermodynamic condition (5 °C -55 °C, with a dwell-time of 60 s and a transfer time of 24 s and mechanical load of 5 kgf (49 N) for 120,000 times simultaneously. The conical-shaped opposing plunger, which was made of nickel-chromium, was initially positioned at the buccal surface. No direct contact was made to the resin restoration. A 5 kgf load was applied to press down on the buccal surface of the tooth. The rod moved 6 mm vertically and 0.3 mm horizontally. The rising speed was 55 mm/s, while the descending speed was 30 mm/s. After the thermo-mechanical loading, the samples were stored in distilled water at room temperature.

3.2.5. SS-OCT imaging

The SS-OCT used in this study was the Santec OCT-2000 (Santec Co., Komaki, Japan). It is a frequency domain OCT system, integrating a high-speed frequency sweeping external cavity. The laser probe power is less than 20 mW. The light source in the system sweeps the wavelengths from 1260 nm to 1360 nm at a scan rate of 20 kHz. The system relies on analyzing the frequency components of backscattered light from the internal structure of an object, thus it creates real-time 2D images. The photo-detected signal is amplified and sent to the computer. The axial resolution of the OCT system is 11 μm in air, which is equivalent to 8 μm in soft tissue and 7 μm in oral hard tissue and resin composite, assuming refractive indices of about $n = 1.5$. The lateral resolution is about 17 μm and the output is an image of 512x1024 pixels (Bakhsh et al., 2011; Makishi et al., 2011).

The imaging depth of the SS-OCT laser through the majority of dental composites is known to be less than 3 mm. Before taking SS-OCT images, the upper 2 mm part of the tooth or composite material was cut off of all the specimens. All the specimens were cut at the top 2 mm of the restoration with a diamond disc (Fig. 12). The hand-held scanning probe connected to the SS-OCT was placed over the top of the restorations and was oriented at a right angle to the occlusal surface of the restoration. The light beam was projected onto the resin restoration and scanned across the area. The first SS-OCT image of the restoration was taken parallel to the bucco-lingual plane of

the cavity at the center of the restoration. After the image was taken, the platform holding the specimen was rotated 15° clockwise, then the next image was taken. Twelve images were taken per each sample (Fig. 12, right end).

3.2.6. Measuring internal adaptation of the specimens on the SS-OCT image

The SS-OCT images were imported into the ImageJ program. It is known that when there is a microgap between two media of different refractive indices, the reflections of light at the interface will be dissimilar (Sadr et al., 2011). The presence of air, which means a microgap between the tooth material and restorative material, is visualized as bright spot on the SS-OCT image. The high signal intensity at the resin-dentin interface created bright spots or clusters (Figs.13 and 14). To measure the imperfect margins of the cavity floor, the length of the bright spots on the cavity floor was measured. The cavity floor part where signal intensity was above the threshold was thought to be imperfect margins. The percentage of imperfect margin (%IM) was defined as the percentage from dividing the sum of portions where signal intensities were above the threshold by the entire length of a floor. If %IM increases, it means that composite restoration has poor internal adaptation. GapAnalyzer, which is a plug-in software for ImageJ, was used to verify the imperfect margin and was the same method used by Bista et al.(Bista et al., 2013). It can show a spot or cluster where the signal intensity was above the threshold as white dots (lower right windows in Figs. 13 and 14).

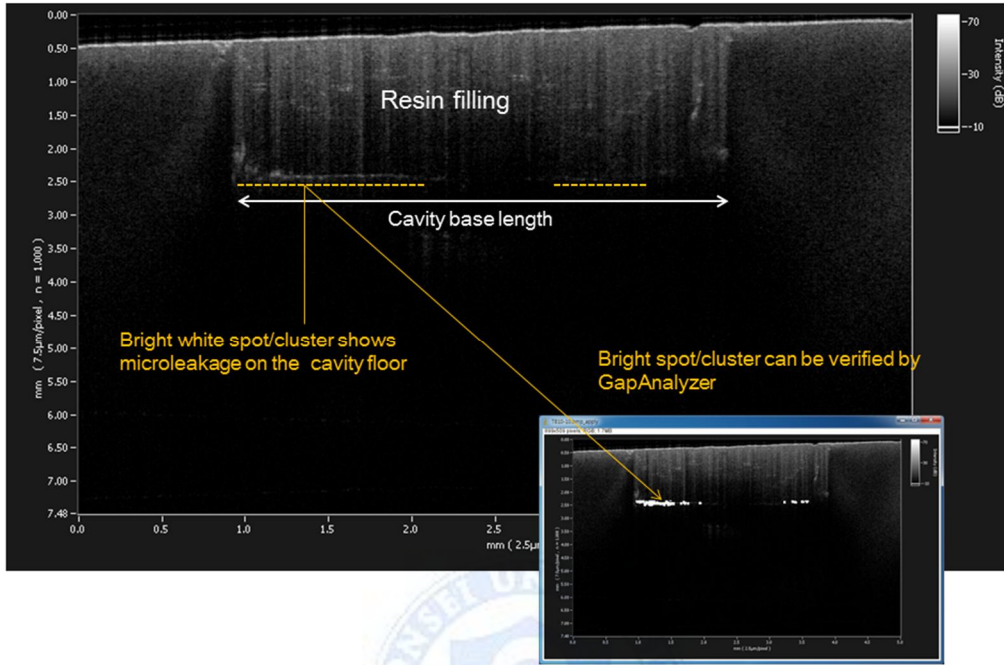


Fig. 13. SS-OCT image of High C-factor cavity with the inset of GapAnalyzer image (Bista et al., 2013)

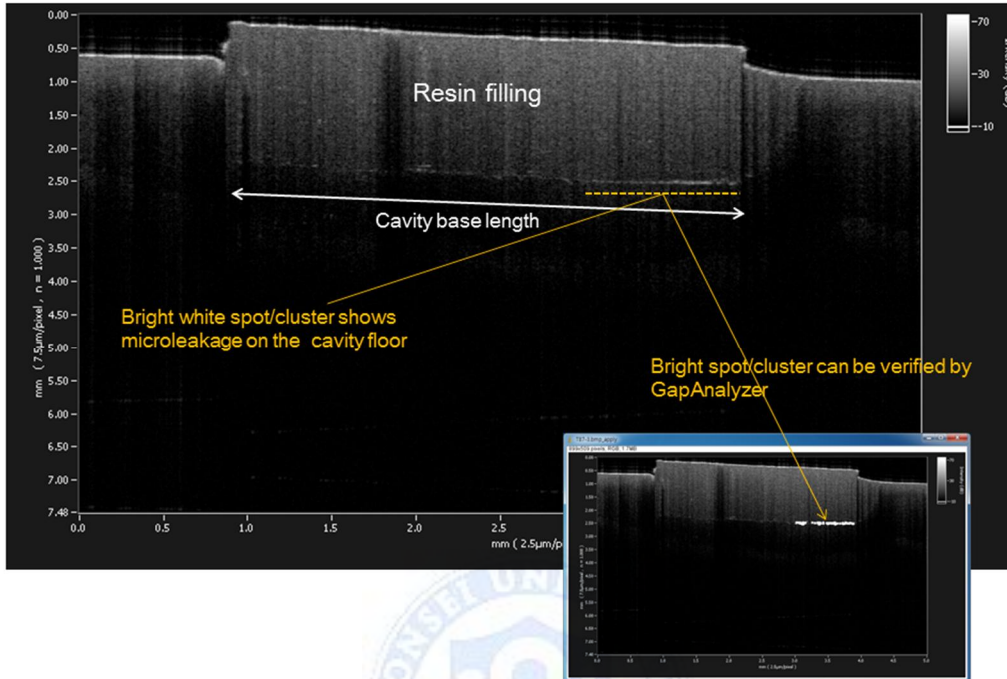


Fig. 14. SS-OCT image of Low C-factor cavity with the inset of GapAnalyzer image

3.2.7. Measuring the linear polymerization shrinkage of resin composite

Polymerization shrinkage strain was measured using a custom-made Linometer (R&B Inc., Daejeon, Korea). Glycerin gel was applied to a metallic disc and a piece of glass slide to prevent adhesion to the resin. Then, 18.85 mm² of resin composite was placed on the thin metallic disc, covered with a glass slide, and positioned into place under constant pressure using a screw. An LED type light-curing unit (Bluephase, Ivoclar Vivadent, Schaan, Liechtenstein) with a power density of 800 mW/cm² was placed 1 mm above the glass slide, and the material was light-cured for 30 s. As the resin composite under the glass slide was cured, it moved the aluminum disk downward. The amount of disk displacement was measured using an eddy current sensor every 0.5 s for a period of 180 s. This measurement was repeated five times for each material and the average was calculated.

3.2.8. Measurement of the polymerization shrinkage force

The polymerization shrinkage force of the resin composite was measured using a custom-made device and software (R&B Inc., Daejeon, Korea). The instrument was driven by a motor and was devised to move a metal bar up and down. The polymerization shrinkage force applied to the acrylic tension rod was measured by a load cell (100 kgf) connected to the bar. The light to polymerize the resin composite sample was projected from beneath the transparent disc. The entire process was controlled by the software made by R&B Inc.

Before connecting the acrylic rod, its surface was roughened with sandpaper (180 grit), treated by adhesive resin (bonding agent, Clearfil SE bond, Kuraray Noritake Dental, Okayama, Japan) and light-cured. For the measurement of the polymerization stress under a zero-compliance condition, 7.07 mm² of resin composite was placed onto an acrylic disc, and the upper acrylic rod was positioned to ensure that the thickness of the specimen was 1 mm and its diameter was 3 mm. Thus, the C-factor ($d/2h$, d : diameter, h : height) was 1.5. The force measurement between the tension rod and the resin composite was set to zero before light curing. Then, the resin composite was light-cured with a light-curing unit (Bluephase, Ivoclar Vivadent, Schaan, Liechtenstein, 800 mW/cm²) for 20 s through the transparent disc. While shrinkage force developed, the displacement of the acrylic tension rod from resin polymerization was restricted for the zero-compliance measurement. In this mode, as soon as the sensor detected the linear displacement of more than 1 mm during the polymerization process, the program in the machine made opposing rod move backward to keep the same distance which had been set at the very beginning. Along with the load-cell signal, the displacement was continuously recorded to the computer every 0.1 s for a period of 180 s. This measurement was repeated five times for each material and calculated for average value.

The polymerization stress under the compliance-allowed condition, using the same amount of resin composite, was also gauged. Before measurements, the setup was switched to compliance-allowed mode in which the acrylic rod could be moved freely according to the resin polymerization. The compliance of the system was 0.3 $\mu\text{m/N}$ when the acrylic rod was used.

After 7.07 mm² of resin composite was placed onto an acrylic disc, the upper acrylic rod was positioned to ensure that the thickness of specimen was 1 mm and its diameter was 3 mm. During the light-curing, shrinkage force caused displacement of the acrylic tension rod which was connected to the load cell. Along with the load-cell signal, the displacement and stress was continuously recorded to the computer every 0.1 s for a period of 180 s. This measurement was repeated five times for each material and calculated for average value.

3.2.9. Statistic analysis

To compare the %IM results between High C-factor and Low C-factor groups, two way ANOVA with Scheffe post hoc test was used. For the comparison of subgroups within each High and Low C-factor group, one way ANOVA with Scheffe analysis was applied. Finally, Pearson correlation test was done among the variables: LS, PS0, PS, %IM of H-CF, %IM of L-CF.

3.3. The results of the third experiment

The percentages of imperfect margin measured by SS-OCT are presented in Table 10. The High C-factor cavity group showed significantly higher %IM than the Low C-factor cavity group ($p < 0.05$). The %IM in the High C-factor cavity turned out to be the following: group 2, group 1 \leq group 4 < group 3, group 5. The %IM in the Low C-factor cavity showed as the following order: group 2, group 4 \leq group 1, group 3 < group 5. The relationships between internal adaptation and polymerization stress or linear polymerization shrinkage are presented in Table 11.

Table 9. Measurements of polymerization shrinkage and stress on resin composites used in this study

Code	Linear polymerization shrinkage (LS, %)	Polymerization stress under the zero-compliance (PS0, MPa)	Polymerization stress under the compliance-allowed (PS, MPa)
FS	1.36 (0.10) ^b	4.70 (0.22) ^a	2.19 (0.12) ^b
CD	1.12 (0.09) ^a	4.20 (0.30) ^a	1.74 (0.15) ^a
AP	2.00 (0.12) ^c	9.47 (0.27) ^c	3.23 (0.22) ^c
TB	1.21 (0.09) ^{a,b}	5.86 (0.22) ^b	2.03 (0.12) ^{a,b}
VB	2.27 (0.11) ^d	8.94 (0.29) ^c	3.46 (0.18) ^c

Polymerization linear shrinkage and polymerization stress are the averaged value of five-time measurements.

Numbers in parenthesis are standard deviations.

Identical superscript represents no statistically significant difference among groups ($p < 0.05$).

Table 10. Percentages of imperfect margin for each group

	FS	CD	AP	TB	VB
High C-factor cavity (H-CF)	30.88(3.74) ^{a,b}	26.97(7.41) ^a	47.69(4.74) ^c	38.02(8.48) ^b	52.81(7.84) ^c
Low C-factor cavity (L-CF)	26.70(2.33) ^a	21.79(2.69) ^b	29.78(3.83) ^a	25.59(3.37) ^{a,b}	38.17(3.13) ^c

Closed bar with asterisk indicates statistically significant difference between High C-factor and Low C-factor (two way ANOVA, $p < 0.05$).

Identical superscript represents no statistically significant difference among groups (compared in each row, one way ANOVA, $p < 0.05$).

Values in the parenthesis represent standard deviations.

Table 11. Pearson Correlations Among Variables

	LS	PS0	PS
%IM in H-CF group	.932	.963	.947
Sig.	0.021	0.009	0.015
%IM in L-CF group	.933	.801	.915
Sig.	0.021	N.S.	0.03

Numbers in the table are r-values.

N.S.: no significant correlation ($p > 0.05$).

III. Discussion

In the first experiment, the 1st null hypothesis was rejected by the results of post thermo-cycling. The 2nd null hypothesis was also rejected because higher values were found for micro-CT than SS-OCT. However, there was a correlation ($r=0.787$) between SS-OCT and micro-CT.

The %DS measurements of micro-CT were lower than those of SS-OCT. It was after thermo-cycling that the results of SS-OCT and micro-CT were compared. That's because it was not known whether silver nitrate infiltration could have an effect on the image of SS-OCT. After thermo-cycling, once all the images of SS-OCT had been taken, silver nitrate could be infiltrated. Silver nitrate was used as the tracer to fill the microgaps and to be detected on X-ray images (De Santis et al., 2005). One of the reasons for this different leakage% of SS-OCT with micro-CT would be silver ions might not infiltrate sufficiently into all of the microgaps between the resin composite and tooth. In the TEM evaluation of nanoleakage, silver nitrate infiltrated very thin tooth specimens (Sano et al., 1995b). For evaluation of marginal leakage, it infiltrated the gap between the cavity and restoration from outside (Sano et al., 1995a). However in our experiment, silver nitrate infiltrated from the pulp space through about 0.5-1mm length of dentinal tubules into the gap under the restoration. It could be trapped in the dentinal tubules in the course of infiltration. This might lower the sensitivity of the identifying microgaps on micro-CT images.

Another cause could be different setting of the threshold for SS-OCT and micro-CT. If the threshold had been set lower, higher leakage % would have been presented. Also, it could be possible reason that the matching images of micro-CT and SS-OCT had not been taken at the same corresponding location. It was not proved that SS-OCT and micro-CT had the same ability to evaluate the internal adaptation. However, the Pearson correlation showed a significant correlation between the two imaging methods (correlation coefficient $r=0.787$, $p<0.01$). Both systems may be used not for the absolute measurement on the imperfections of restorations, but for relative comparison of the restorations.

The %DS was found to be $\text{Group 3} \leq \text{Group 4} < \text{Group 1} \leq \text{Group 2}$ in both SS-OCT and micro-CT. This result shows that two-step etch-and-rinse adhesives demonstrate inferior durability after

the aging process. This result was consistent with a previous report on the effects of acid etching on dentin (Shirai et al., 2005). All of the margins and cavity floors were located on the dentin in our experiments. Etching on the dentin surface may have left dissolved calcium phosphates that were not rinsed away. These embedded calcium phosphates are very unstable (Yoshida et al., 2001). Moreover, excessive etching clears away hydroxyapatite crystals from the collagen fibrils. The exposed dentinal collagen is known to be very vulnerable to internal hydrolytic degradation (Van Meerbeek et al., 2011). Thus, excessive etching might have happened during the process. Technical difficulties are another pitfall associated with the proper handling of etch-and-rinse adhesive systems (Pashley et al., 2011). As all the cavity margins were located on the dentin, peripheral sealing by enamel etching would not have worked (Hashimoto et al., 2002). In addition, groups 1 and 2 showed relatively higher standard deviations than groups 3 and 4. The observed higher standard deviation could also be attributed to the different degrees of wetness on the dentin surface.

Micro-CT and SS-OCT have their own characteristics as a tool for evaluation. Micro-CT has no limitation for evaluating the restoration in terms of cavity depth. However, SS-OCT has depth limitations. Even though SS-OCT shows very clear images within the penetrating depth of the laser, it cannot be used in deep cavities and fillings. The cavity depth in our experiment was 2 mm because the imaging depth of SS-OCT systems had been reported to be in the range of 2-3 mm (Shimada et al., 2010). SS-OCT images were generally clear and the high-intensity white spots or clusters could easily be identified on the image. In some cases, imprecise spots and indistinct parts were observed. It would be ideal to evaluate the images with a predefined signal intensity threshold for the defect. However, defining a SS-OCT threshold for the microgap was very complicated because the signal intensity was affected by the light intensity, scattering, attenuation and transmittance properties of the material. When light passes through a material such as resin composite, the light is scattered and attenuated with depth. The light transmittance is different for resin composite depending on its composition. Therefore, it was impossible to compare OCT signal intensity levels using a single constant threshold (Bakhsh et al., 2011). A relative comparison was possible depending on the experimental conditions. Bista et al. suggested that an automated signal analysis algorithm could be utilized to detect the high signal intensity at the

interface (Bista et al., 2013).

In the second experiment, GFIM%, MPFIM%, and DPFIM% turned out to be significantly higher than BWIM% and LWIM%. TIM% was different among groups. These findings indicated that the first and second null hypotheses were rejected.

GFIM% was recorded relatively higher than BWIM% and LWIM% in the proximal box. It might be due to the following reasons. First, the occluso-gingival dimension of the proximal box was larger than the bucco-lingual dimension of the box. The dimensions were approximately 6 mm for the occluso-gingival height and 3.5 mm for the bucco-lingual width. As the bulk resin polymerized, polymerization shrinkage could be greater in the direction of the occluso-gingival axis than that of the bucco-lingual axis. This could lead to a higher IM% at the interface of the gingival floor. While measuring imperfect margins at the restoration interfaces, imperfections were often found around the axiofaciogingival or axiolinguogingival point-angles of the proximal box. This would be because these two point-angles were the places where two directional vectors of force were exerted: toward the occlusal surface and toward the buccal/lingual surface. Second, the buccal and lingual walls had their own portion of the enamel margin. There could be stronger bonding with the enamel part of the cavity where little microleakage along the enamel margin was found on the micro-CT images. After resin polymerization, the composite restoration might have ended up with a strong bond at the occlusal margin and a weak bond at the cervical margin. Intact enamel margins could help to lessen the IM% of the buccal and lingual wall. Third, dentinal tubules on a deep cavity floor have different characteristics from those of outer superficial dentin. The tubule diameters near the pulpo-dentinal junction (PDJ) are larger, the distance between tubule centers is half that between tubule centers at the DEJ, and peritubular dentin is either diminished in thickness or absent (Fosse et al., 1992). At the PDJ, the volume of the fluid filled tubule lumens approaches 80% (Pashley et al., 2002). Therefore, the dentin at this area is known to be more permeable and wetter than the dentin at the DEJ (Pashley, 1996). This is a poor condition to achieve good dentin bonding, especially with an etch-and-rinse system like XP-bond used in this experiment (Moll and Haller, 2000). For this reason, the gingival and pulpal floors of the cavity could be more unfavorable to dentin bonding than the occlusal portion of the buccal and lingual

walls.

The polymerization shrinkage and stress are thought to be a major factor for the different IM% of the groups. The different resin composites have their own characteristics of polymerization shrinkage. Groups 2 and 3, where flowable bulk-fill composite resins were used, showed greater IM% on the gingival and pulpal floors. Linear polymerization shrinkages were shown to be in the increasing order of TB, SF, Z3 < SD < VB. The result of polymerization shrinkage stress turned out to be in the increasing order of SF, TB ≤ Z3 < SD < VB. Both VB and SD, which showed high linear polymerization shrinkage and stress, led to higher IM%.

The non-flowable bulk-fill resins, TB and SF, showed better internal adaptation than the flowable bulk-fill resins. The manufacturer of TB insisted that TB include an initiator named Ivocerin that works as a polymerization booster. TB also contains low elastic modulus fillers that work as a shrinkage stress reliever. SF uses sonic energy for placement of the composite. It is known that SF has a special modifier which can be activated by sonic wave. Once activated by sonic energy, the viscosity of SF can be reduced to have a rheological property for adaptation. When the polymerization shrinkage is similar, it is known that the material with a low viscosity shows better marginal adaptation (Peutzfeldt and Asmussen, 2004). What had been observed in samples of the SF group were, however, small bubbles inside the resin restoration. That could be due to the vibration of the resin composite by sonic energy. The bubbles may act as pros and cons. They may act as a stress reliever. However, the bubbles may increase IM% if they happened to occur at the interface between the composite and tooth.

In the third experiment, higher %IM (inferior internal adaptation) was found in the High C-factor cavity than in the Low C-factor cavity (Table 10). Internal adaptation was different among some groups in both the High C-factor and the Low C-factor cavities (Table 10). Therefore the first and second hypotheses were rejected. Internal adaptation (%IM) was also different depending on the composite materials in High and Low C-factor groups. A non-flowable bulk-filled composite (TB) showed comparable results with those of a hybrid resin composite resin placed in increments. The latest generations of the flowable bulk-fill composite have claimed to have higher filler content and increased mechanical properties. In this study, however, a flowable bulk-fill

composite (VB) did not show low polymerization shrinkage and stress. It was also found that VB showed relatively high %IM in the High C-factor and Low C-factor cavities. Among the two composites investigated in this study, the non-flowable bulk fill composite may be preferable to the flowable bulk fill. Nonetheless, it appears that for a high C-factor large cavity, incremental placement of conventional composite has advantage over the bulk placement of a bulk fill composite.

There was no significant correlation between internal adaptation and polymerization stress in the Low C-factor cavity under the zero-compliance condition (Table 11), therefore the third null hypotheses was partially rejected. While resin composite can shrink relatively freely in a low C-factor cavity, its shrinkage in a high C-factor cavity is more restricted by adhesion to the cavity walls and can have a stronger effect on internal adaptation. In other words, polymerization stress has different vectors and force depending on its cavity form (Witzel et al., 2007). The polymerization shrinkage stress under the zero-compliance condition was higher than that under the compliance-allowed condition (Table 9). The most frequently used setup for measuring polymerization stress is composed of placing the resin composite between two flat surfaces of a universal testing machine. To make a zero (near-zero) compliance condition, the height of the composite disc is constantly monitored and kept by a feedback system. If any displacement of the disc is detected, the cross-head will counteract in the opposite direction, keeping the height constant (Choi et al., 2000; Feilzer et al., 1987). However, it should be considered that if the compliance were absolutely restricted, the stress would theoretically increase to infinity. So, the term of “near-zero compliance system” would be more appropriate. In terms of the compliance, the concern was the compliance of the tooth specimen and that of the measuring system. Considering that the elastic modulus of dentin ranges between 6 and 17 GPa, it is thought that there is some compliance in the dental structure (Miura et al., 2009). In the experiment with the non-feedback system, the stress values were lower than those with a feedback system, which is in line with previous reports (Bouschlicher et al., 1997; Braga and Ferracane, 2004; Miguel and de la Macorra, 2001). However, as with any method, measuring contraction stress by a universal testing machine (UTM) can have limitations. The main shortcoming is that the stress can be recorded only in the long axis of the specimen, rather than under a tri-axial condition (Laughlin et al., 2002).

The correlation between internal adaptation in the Low C-factor cavity and polymerization stress under the zero-compliance condition was not significant (Table 11). It could be due to the mismatch between the compliance of the stress measuring system (UTM) and that of the tooth cavity. While the polymerization stress under a zero-compliance condition meant that the stress was measured under a condition where no compliance or composite strain was allowed in the system, the composite in the Low C-factor cavity could more freely strain. Laughlin et al. indicated that the system compliance and sample geometry had a profound effect on the polymerization stress (Laughlin et al., 2002). In other studies, the compliance of the tooth structure was shown to be much higher than that of some rigid testing systems (Alster et al., 1997; Feilzer et al., 1987). There was a chance that the polymerization stress value measured under the zero-compliance condition could be much higher than the actual stress developed in the low C-factor cavity. In line with this assumption, other works also reported that the polymerization stress under a zero-compliance condition could be higher than the actual polymerization stress (Braga et al., 2005; Laughlin et al., 2002; Lee et al., 2007). On the other hand, in the High C-factor cavity, polymerization stress in zero-compliance could be a predictive factor for internal adaptation. It should be considered that polymerization stress under the zero-compliance condition increased exponentially as the C-factor of a cavity increased (Feilzer et al., 1987, 1993; Witzel et al., 2007).

A more interesting finding in this study was that polymerization stress under the compliance-allowed condition could be applicable to both High and Low C-factor cavities. Previous researches showed various compliance values in tensiometer and teeth (Goncalves et al., 2008; Laughlin et al., 2002; Lee et al., 2007). Recently, Rodrigues et al. calculated the compliance of Class I cavities using the finite element method (Rodrigues et al., 2014). They showed diverse compliances of prepared tooth cavities depending on different shapes and dimensions. The results of the paper indicated that the calculated compliance in a Class I cavity turned out to be 0.204~0.863 $\mu\text{m}/\text{N}$. In another study, the cuspal compliance of an MOD cavity was 3.34 $\mu\text{m}/\text{N}$ (Lee et al., 2007). This could be one of the reasons that the polymerization stress under the compliance-allowed condition showed relationship with internal adaptation under both C-factor conditions. Other studies utilizing the compliance-allowed system reported a direct relationship between polymerization stress and the volume (Bouschlicher et al., 1997; Miguel and de la Macorra, 2001; Watts et al.,

2003; Watts and Satterthwaite, 2008). Witzel et al. explained that there was not any correlation between stress and specimen volume when polymerization stress under a zero-compliance was adopted (Witzel et al., 2007).

Linear polymerization shrinkage was measured with a linometer using the same method as reported by de Gee et al. (de Gee et al., 1993). The shrinkage value should be considered as a relative comparison depending on the volume of the specimen, not an absolute measurement. In this experiment, it was interesting that the linear polymerization shrinkage percentage showed a similar trend as that of polymerization stress under the compliance-allowed condition. It was also noticeable that a significant relationship was found between %IM and linear polymerization shrinkage under both C-factor conditions (Table 11). It is known that a low volumetric shrinkage does not necessarily correspond to a low polymerization stress development (Boaro et al., 2010b). According to the linear elastic model, the increment in shrinkage stress would be proportional to the product of the increase in volumetric shrinkage by the increment in the material's elastic modulus (Feilzer et al., 1990). Polymerization stress was reported to have shown a strong direct correlation with shrinkage and an inverse correlation with elastic modulus (Goncalves et al., 2010). When there is more systemic compliance, polymerization shrinkage stress could be much more governed by polymerization shrinkage than elastic modulus (Goncalves et al., 2010; Lee et al., 2007). On the other hand, the reduced compliance of the tooth substrate in a High C-factor cavity could intensify the influence of the composite's elastic modulus on polymerization stress (Goncalves et al., 2010; Goncalves et al., 2008). It would mean that modulus of elasticity of the resin composite would have more effect on the polymerization stress in a High C-factor cavity than in a Low C-factor cavity. Boaro et al. found in their experiment that a low compliance system increases the influence of composite stiffness on polymerization stress development (Boaro et al., 2010a).

Flow, which may be one of the factors that affect the polymerization stress, can result in a relief of internal stresses to reduce polymerization stress (Davidson and de Gee, 1984). Flow was known to be influenced by the structure of the individual molecules, cross-linking of the molecules, the filler/matrix interfacial characteristics, reaction kinetics, and cavity configuration. It was reported

that the stress relaxation caused by flow is sufficient to maintain the consistency if the C-factor of a restoration is less than one (Miguel and de la Macorra, 2001). The choice of composite material and cavity form determined the flow features of composite restoration. In this experiment, flow could not be measured during the polymerization process. The polymerization stress under the compliance-allowed condition showed lower shrinkage stress, which reflected the effect of flow.

To identify leakages on digitalized image, a threshold should be set up. How to set a threshold level can be somewhat subjective. However, once it was set, imperfective margin percentage on each sample could be calculated objectively. These methods made it possible to compare internal adaptations relatively. Internal adaptation was thought to be different depending on the dentin adhesive, filling material, cavity configuration and the location of the interface between the composite and tooth cavity.

IV. Conclusion

Micro-CT and SS-OCT could be useful non-destructive methods for evaluation of internal adaptation. Measured imperfective margins% in micro-CT showed different values to those of SS-OCT, however, these two methods were relatively highly correlated. Self-etching adhesive systems showed fewer defective spots than etch-and-rinse adhesive systems in class I cavity.

At the gingival floor of the proximal box and pulpal floor of the cavity, flowable bulk-fill resin showed an inferior internal adaptation when compared with non-flowable ones. For Class II resin restorations, bulk-filling material of the non-flowable type could be preferable to flowable type ones. Polymerization shrinkage and stress, which was measured under the compliance-allowed setup, showed some relation to the internal adaptation.

Within the limitations of the present study, it was shown that a higher imperfect margin percentage was found in the cavities of the High C-factor group. Internal adaptation was different depending on the composite material. Internal adaptations both in the High and Low C-factor

cavities are correlated with polymerization stress measured under the compliance-allowed condition. In the Low C-factor cavity group, the polymerization shrinkage stress measured under the zero-compliance condition did not show a significant correlation to internal adaptation.

References

- Aggarwal V, Singla M, Yadav S, Yadav H (2014). Effect of flowable composite liner and glass ionomer liner on class II gingival marginal adaptation of direct composite restorations with different bonding strategies. *J Dent* 42(5): 619-625.
- Alani AH, Toh CG (1997). Detection of microleakage around dental restorations: a review. *Oper Dent* 22(4): 173-185.
- Alster D, Feilzer AJ, de Gee AJ, Davidson CL (1997). Polymerization contraction stress in thin resin composite layers as a function of layer thickness. *Dent Mater* 13(3): 146-150.
- Bakhsh TA, Sadr A, Shimada Y, Tagami J, Sumi Y (2011). Non-invasive quantification of resin-dentin interfacial gaps using optical coherence tomography: validation against confocal microscopy. *Dent Mater* 27(9): 915-925.
- Bista B, Sadr A, Nazari A, Shimada Y, Sumi Y, Tagami J (2013). Nondestructive assessment of current one-step self-etch dental adhesives using optical coherence tomography. *J Biomed Opt* 18(7): 76020.
- Boaro LC, Goncalves F, Braga RR (2010a). Influence of the bonding substrate in dental composite polymerization stress testing. *Acta Biomater* 6(2): 547-551.
- Boaro LC, Goncalves F, Guimaraes TC, Ferracane JL, Versluis A, Braga RR (2010b). Polymerization stress, shrinkage and elastic modulus of current low-shrinkage restorative composites. *Dent Mater* 26(12): 1144-1150.
- Bouschlicher MR, Vargas MA, Boyer DB (1997). Effect of composite type, light intensity, configuration factor and laser polymerization on polymerization contraction forces. *Am J Dent* 10(2): 88-96.
- Braga RR, Ballester RY, Ferracane JL (2005). Factors involved in the development of polymerization shrinkage stress in resin-composites: a systematic review. *Dent*

Mater 21(10): 962-970.

- Braga RR, Boaro LC, Kuroe T, Azevedo CL, Singer JM (2006). Influence of cavity dimensions and their derivatives (volume and 'C' factor) on shrinkage stress development and microleakage of composite restorations. *Dent Mater* 22(9): 818-823.
- Braga RR, Ferracane JL (2004). Alternatives in polymerization contraction stress management. *J Appl Oral Sci* 12(spe): 1-11.
- Braga RR, Hilton TJ, Ferracane JL (2003). Contraction stress of flowable composite materials and their efficacy as stress-relieving layers. *J Am Dent Assoc* 134(6): 721-728.
- Campos EA, Ardu S, Lefever D, Jasse FF, Bortolotto T, Krejci I (2014). Marginal adaptation of class II cavities restored with bulk-fill composites. *J Dent* 42(5): 575-581.
- Choi KK, Condon JR, Ferracane JL (2000). The effects of adhesive thickness on polymerization contraction stress of composite. *J Dent Res* 79(3): 812-817.
- Chuang SF, Jin YT, Liu JK, Chang CH, Shieh DB (2004). Influence of flowable composite lining thickness on Class II composite restorations. *Oper Dent* 29(3): 301-308.
- Davidson CL, de Gee AJ (1984). Relaxation of polymerization contraction stresses by flow in dental composites. *J Dent Res* 63(2): 146-148.
- de Gee AF, Feilzer AJ, Davidson CL (1993). True linear polymerization shrinkage of unfilled resins and composites determined with a linometer. *Dent Mater* 9(1): 11-14.
- De Santis R, Mollica F, Prisco D, Rengo S, Ambrosio L, Nicolais L (2005). A 3D analysis of mechanically stressed dentin-adhesive-composite interfaces using X-ray micro-CT. *Biomaterials* 26(3): 257-270.
- Eick JD, Welch FH (1986). Polymerization shrinkage of posterior composite resins and its possible influence on postoperative sensitivity. *Quintessence Int* 17(2): 103-111.
- Feilzer AJ, De Gee AJ, Davidson CL (1987). Setting stress in composite resin in relation to configuration of the restoration. *J Dent Res* 66(11): 1636-1639.
- Feilzer AJ, De Gee AJ, Davidson CL (1990). Quantitative determination of stress

- reduction by flow in composite restorations. *Dent Mater* 6(3): 167-171.
- Feilzer AJ, de Gee AJ, Davidson CL (1993). Setting stresses in composites for two different curing modes. *Dent Mater* 9(1): 2-5.
- Fosse G, Saele PK, Eide R (1992). Numerical density and distributional pattern of dentin tubules. *Acta Odontol Scand* 50(4): 201-210.
- Goncalves F, Azevedo CL, Ferracane JL, Braga RR (2011). BisGMA/TEGDMA ratio and filler content effects on shrinkage stress. *Dent Mater* 27(6): 520-526.
- Goncalves F, Kawano Y, Braga RR (2010). Contraction stress related to composite inorganic content. *Dent Mater* 26(7): 704-709.
- Goncalves F, Pfeifer CS, Meira JB, Ballester RY, Lima RG, Braga RR (2008). Polymerization stress of resin composites as a function of system compliance. *Dent Mater* 24(5): 645-652.
- Hashimoto M, Ohno H, Sano H, Tay FR, Kaga M, Kudou Y, et al. (2002). Micromorphological changes in resin-dentin bonds after 1 year of water storage. *J Biomed Mater Res* 63(3): 306-311.
- Ilie N, Bucuta S, Draenert M (2013). Bulk-fill resin-based composites: an in vitro assessment of their mechanical performance. *Oper Dent* 38(6): 618-625.
- Jeong JH, Park SH (2014). Comparison of marginal adaptation in flowable and non-flowable bulk fill resin based composites. Yonsei University, Seoul, Korea M.S. Thesis.
- Kim HJ, Park SH (2014). Measurement of the internal adaptation of resin composites using micro-CT and its correlation with polymerization shrinkage. *Oper Dent* 39(2): E57-70.
- Kwon OH, Kim DH, Park SH (2010). The influence of elastic modulus of base material on the marginal adaptation of direct composite restoration. *Oper Dent* 35(4): 441-447.
- Kwon OH, Park SH (2012). Evaluation of internal adaptation of dental adhesive restorations using micro-CT. *Restor Dent Endod* 37(1): 41-49.
- Laughlin GA, Williams JL, Eick JD (2002). The influence of system compliance and sample geometry on composite polymerization shrinkage stress. *J Biomed Mater Res* 63(5): 671-678.

- Lee SH, Chang J, Ferracane J, Lee IB (2007). Influence of instrument compliance and specimen thickness on the polymerization shrinkage stress measurement of light-cured composites. *Dent Mater* 23(9): 1093-1100.
- Makishi P, Shimada Y, Sadr A, Tagami J, Sumi Y (2011). Non-destructive 3D imaging of composite restorations using optical coherence tomography: marginal adaptation of self-etch adhesives. *J Dent* 39(4): 316-325.
- Meng Z, Yao XS, Yao H, Liang Y, Liu T, Li Y, et al. (2009). Measurement of the refractive index of human teeth by optical coherence tomography. *J Biomed Opt* 14(3): 034010.
- Miguel A, de la Macorra JC (2001). A predictive formula of the contraction stress in restorative and luting materials attending to free and adhered surfaces, volume and deformation. *Dent Mater* 17(3): 241-246.
- Miura J, Maeda Y, Nakai H, Zako M (2009). Multiscale analysis of stress distribution in teeth under applied forces. *Dent Mater* 25(1): 67-73.
- Moll K, Haller B (2000). Effect of intrinsic and extrinsic moisture on bond strength to dentine. *J Oral Rehabil* 27(2): 150-165.
- Moorthy A, Hogg CH, Dowling AH, Grufferty BF, Benetti AR, Fleming GJ (2012). Cuspal deflection and microleakage in premolar teeth restored with bulk-fill flowable resin-based composite base materials. *J Dent* 40(6): 500-505.
- Pashley DH (1996). Dynamics of the pulpo-dentin complex. *Crit Rev Oral Biol Med* 7(2): 104-133.
- Pashley DH, Pashley EL, Carvalho RM, Tay FR (2002). The effects of dentin permeability on restorative dentistry. *Dent Clin North Am* 46(2): 211-245, v-vi.
- Pashley DH, Tay FR, Breschi L, Tjaderhane L, Carvalho RM, Carrilho M, et al. (2011). State of the art etch-and-rinse adhesives. *Dent Mater* 27(1): 1-16.
- Peutzfeldt A, Asmussen E (2004). Determinants of in vitro gap formation of resin composites. *J Dent* 32(2): 109-115.
- Rodrigues FP, Lima RG, Muench A, Watts DC, Ballester RY (2014). A method for calculating the compliance of bonded-interfaces under shrinkage: validation for Class I cavities. *Dent Mater* 30(8): 936-944.
- Roggendorf MJ, Kramer N, Appelt A, Naumann M, Frankenberger R (2011). Marginal

- quality of flowable 4-mm base vs. conventionally layered resin composite. *J Dent* 39(10): 643-647.
- Sadr A, Shimada Y, Mayoral JR, Hariri I, Bakhsh TA, Sumi Y (2011). Swept source optical coherence tomography for quantitative and qualitative assessment of dental composite restorations. *Proceedings of SPIE* 7884: 78840C.
- Sano H, Takatsu T, Ciucchi B, Horner JA, Matthews WG, Pashley DH (1995a). Nanoleakage: leakage within the hybrid layer. *Oper Dent* 20(1): 18-25.
- Sano H, Yoshiyama M, Ebisu S, Burrow MF, Takatsu T, Ciucchi B, et al. (1995b). Comparative SEM and TEM observations of nanoleakage within the hybrid layer. *Oper Dent* 20(4): 160-167.
- Senawongse P, Pongprueksa P, Harnirattisai C, Sumi Y, Otsuki M, Shimada Y, et al. (2011). Non-destructive assessment of cavity wall adaptation of class V composite restoration using swept-source optical coherence tomography. *Dent Mater J* 30(4): 517-522.
- Shimada Y, Sadr A, Burrow MF, Tagami J, Ozawa N, Sumi Y (2010). Validation of swept-source optical coherence tomography (SS-OCT) for the diagnosis of occlusal caries. *J Dent* 38(8): 655-665.
- Shirai K, De Munck J, Yoshida Y, Inoue S, Lambrechts P, Suzuki K, et al. (2005). Effect of cavity configuration and aging on the bonding effectiveness of six adhesives to dentin. *Dent Mater* 21(2): 110-124.
- Uno S, Tanaka T, Inoue S, Sano H (1999). The influence of configuration factors on cavity adaptation in compomer restorations. *Dent Mater J* 18(1): 19-31.
- Van Meerbeek B, Yoshihara K, Yoshida Y, Mine A, De Munck J, Van Landuyt KL (2011). State of the art of self-etch adhesives. *Dent Mater* 27(1): 17-28.
- Watts DC, Marouf AS, Al-Hindi AM (2003). Photo-polymerization shrinkage-stress kinetics in resin-composites: methods development. *Dent Mater* 19(1): 1-11.
- Watts DC, Satterthwaite JD (2008). Axial shrinkage-stress depends upon both C-factor and composite mass. *Dent Mater* 24(1): 1-8.
- Witzel MF, Ballester RY, Meira JB, Lima RG, Braga RR (2007). Composite shrinkage stress as a function of specimen dimensions and compliance of the testing system. *Dent Mater* 23(2): 204-210.

Yoshida Y, Van Meerbeek B, Nakayama Y, Yoshioka M, Snauwaert J, Abe Y, et al. (2001). Adhesion to and decalcification of hydroxyapatite by carboxylic acids. *J Dent Res* 80(6): 1565-1569.



국문요약

micro-CT와 SS-OCT를 이용한 복합 레진에서의 내부 적합성 평가

연세대학교 대학원 치의학과

지도교수 박성호



I. 서론

내부 적합성은 치아 내면에서 수복물이 치아에 얼마나 잘 적합되어 있는냐를 의미하며, 수복물의 pulpal floor에서 미세간극을 측정하여 평가할 수 있다. 내부적합성의 비파괴적 검사 방법으로 micro-CT로 치아단면을 촬영하여, 수복물의 내면적합성 평가를 할 수 있다. 다른 방법으로, OCT (optical coherence tomography)를 생체내 단면촬영을 위해 사용하기 시작했다. 이 논문의 주제는 여러 가지 다른 모양의 와동에서, 여러가지 종류의 복합레진의 내부적합성의 평가이다. 이 논문은 micro-CT와 SS-OCT를 사용하여 복합레진의 내부적합성을 평가하는 세가지 다른 실험으로 구성되어 있다.

II. 재료, 방법 및 결과

실험 1

재료 및 방법

12개의 우치의 순면에 각각 2개의 디스크 모양의 와동을 형성하였다. 24개의 와동은 상아질 접착제에 따라 4개의 그룹으로 나누었다: 1) 3단계 etch-and-rinse 접착제, 2) 2단계 etch-and-rinse 접착제, 3) 2단계 self-etch 접착제, 그리고 4) one-step self-etch adhesive. 상아질 접착제의 적용 후에, 각 와동은 복합레진으로 충전하였다. 모든 수복물은 thermo-cycling 과정을 거친 후에, 수복물 마다 Santec OCT-2000™ (Santec Co., Komaki, Japan)을 이용하여, 8장의 SS-OCT 이미지를 촬영하였다. 내부적합성은 micro-CT (Skyscan, Aartselaar, Belgium)를 통해서도 평가 되었다. 이미지 분석은 각 이미지에서 defectivce spot의 백분율 (%DS)를 계산하여 결과를 비교하였다. 각 그룹의 결과는 one way ANOVA와 Duncan analysis 로 95% 유의수준에서 검정하였다. SS-OCT와 micro-CT의 측정값은 paired t-test로 비교하고, 결과의 연관성은 Pearson correlation test로 95% 신뢰수준에서 평가하였다.

결과

Thermo-cycling 후에 %DS 는 SS-OCT 와 micro-CT 결과 모두에서 $\text{Group 3} \leq \text{Group 4} < \text{Group 1} \leq \text{Group 2}$ 으로 나타났다. micro-CT 의 %DS 가 SS-OCT 의 %DS 보다 낮은 값을 보였다 ($p < 0.05$). SS-OCT 와 micro-CT 의 Pearson correlation coefficient 는 $r = 0.787$ ($p < 0.05$)로 나타났다.

실험 2

재료 및 방법

40개의 발치된 영구치에 MOD 와동을 형성한 후, 8개씩 5개의 그룹으로 나누었다. 같은 한가지 상아질 접착제를 바른 후 다음 복합레진으로 수복하였다: Group 1- Filtek Z350 (3M); Group 2- SDR (Dentsply) + Z350; Group 3- Venus Bulk Fill (Heraeus Kulzer) + Z350; Group 4- Tetric N-ceram bulkfill (Ivoclar Vivadent); and Group 5- SonicFill (Kerr). Thermo-mechanical load cycling 후, micro-CT 이미지를 촬영하였다. 내부적합성을 imperfect margin 백분율(IM%)로 측정하였다. IM%는 전체 변연길이에 대한 결함부위의 백분율로 정의하였다. micro-CT 이미지에서, 5군데 변연의 IM%를 측정하여 비교하였다. 선수축율과 중합수축력을 각각의 복합레진에서 측정하였다. 중합수축력과 IM%와의 관련성을 확인하기 위해, 선형 회기분석을 사용하였다.

결과

와동 floor에서 IM%는 와동 wall의 IM% 보다 높게 나타났다. IM%은 Groups 4, 5 ≤ Groups 1, 2 ≤ Group 3 으로 나타났다 ($p < 0.05$). 선형 회기분석에서, 중합수축력과 IM%는 $R^2=0.636$ 로, 선수축률과 IM% 사이에서는 $R^2=0.618$ 으로 나타났다.

실험 3

재료 및 방법

100개의 건전한 사랑니에 3mm직경의 원통형 와동을 2가지 깊이로 형성하였다; 4mm (High C-factor: H-CF) 혹은 1mm (Low C-factor: L-CF). 상아질 접착제 (Clearfil SE One, Kuraray Noritake, Japan) 를 바른 후에, 복합레진을 2층의 적층법으로 다음 세가지 서브그룹에서 적용하였다: Filtek Supreme (FS, 3M ESPE); Charisma Diamond (CD, Heraeus Kulzer); Amelogen Plus (AP, Ultradent). 다음 두가지 서브그룹은 한번에 충전하였다: Tetric EvoCeram Bulk Fill (TB, Ivoclar Vivadent), Venus Bulk Fill (VB, Heraeus Kulzer). Thermo-mechanical load-cycles 후에 imperfect margin 백분율 (%IM)을 SS-OCT 이미지를

촬영하여 계산하고 그룹별로 비교하였다. %IM는 선수축율(LS) 과의 관련성, zero-compliance 조건 하에서의 중합수축력 (PS0)과의 관련성, compliance-allowed 조건하의 중합수축력 (PS)과의 관련성을 평가하였다.

결과

H-CF의 %IM와 L-CF의 %IM는 유의성 있게 다르게 나타났다. H-CF의 %IM는 groups 2, $1 \leq \text{group } 4 < \text{groups } 3, 5$ 으로, L-CF의 %IM는 groups 2, $4 \leq \text{groups } 1, 3 < \text{group } 5$ 으로 나타났다. PS0 와 L-CF의 %IM 경우만 제외하고, 중합수축율과 중합수축력은 %IM과 유의성있는 상관관계를 나타내었다.

III. 결론

Micro-CT와 SS-OCT는 복합레진 수복물의 내부적합성을 평가하는데 비파괴적 방법으로 사용 될 수 있다. Micro-CT로 측정된 imperfect margin 백분율은 SS-OCT의 백분율과 다른 값을 보였다. 하지만 이들 두 가지 방법은 높은 상관관계가 있었다. I급 와동에서 self-etching 상아질 접착제는 etch-and-rinse 접착제보다 defective spot이 적게 나타났다.

Proximal box의 gingival floor와 와동의 pulpal floor에서 flowable bulk-fill 레진은 non-flowable bulk-fill 레진보다 낮은 내부적합성을 보였다. II급 와동에서 복합레진 수복 시 non-flowable bulk-fill 레진으로 수복한 경우에 flowable bulk-fill 레진으로 수복한 경우보다 내부적합성에서 더 나은 결과를 보였다. 중합수축량 및 compliance-allowed 조건하에서 측정된 중합수축력은 내부적합성과 관련성을 보여주었다.

이번 실험조건에서, 높은 C-factor 와동에서 낮은 C-factor 와동에서 보다 낮은 내부적합성을 보여주었다. 내부적합성은 복합레진에 따라 다르게 나타났다. 높은 C-factor와 낮은 C-factor 에서의 내부적합성은 compliance-allowed 조건하에서의 중합수축력과 관련성을 보였다. 낮은 C-factor 에서, 내부적합성은 zero-compliance

조건하에서의 중합수축력과 관련성을 나타내지 않았다.



핵심 되는 말

내부적합성, micro-CT, SS-OCT, optical coherence tomography, C-factor, 중합수축량,
중합수축력, compliance, bulk-fill 복합레진, 상아질 접착제